

# A proxy of subsurface Chlorophyll-a in shelf waters: use of density profiles and the below mixed layer depth (BMLD)

Arianna Zampollo<sup>1,\*</sup>, Thomas Cornulier<sup>1</sup>, Rory O'Hara Murray<sup>2</sup>, Jacqueline Fiona Tweddle<sup>1</sup>, James Dunning<sup>1</sup>, Beth E. Scott<sup>1</sup>

<sup>1</sup> School of Biological Sciences, University of Aberdeen, Aberdeen, AB24 2TZ, UK

<sup>2</sup> Marine Scotland Science, Aberdeen, AB11 9DB, UK

Correspondence to: Arianna Zampollo (zampolloarianna@gmail.com)

## Abstract

Primary production dynamics are strongly associated with vertical density profiles, ~~which dictate the depth of stratification and mixed layers in shelf waters~~. Climate change and artificial structures (e.g. windfarms) are likely to modify the strength of stratification and ~~the~~ vertical distribution of nutrient fluxes, especially in shelf seas where ~~fine scale processes are important drivers, affecting the balance between mixing and stratification~~ define the vertical distribution of phytoplankton. To understand the effect of physical changes on primary production, identifying the linkage between density and ~~phytoplankton~~ chlorophyll-a (Chl-a) profiles is essential. Here, the ~~ecological~~ biological relevance of eight density ~~layers~~ levels (DLs) ~~obtained by multiple methods that define~~ characterizing three different portions of the pycnocline (~~above~~ start, centre, ~~below~~ end) was evaluated to ~~identify~~ find a valuable proxy for subsurface Chlorophyll-a (Chl-a  $\text{mg}\cdot\text{m}^{-3}$ ) concentrations ~~in stratified conditions~~. The ~~associations~~ vertical distribution of subsurface Chl-a with surface and deep mixing were investigated. Chl-a maximum (C<sub>MD</sub>) was compared to the depth of DLs by hypothesizing ~~the~~ their occurrence at the same depth ~~of any DL and the maximum Chl-a layer (DMC)~~ using Spearman correlation, linear regression, and a Major Axis analysis. Out of 1237 observations of the water column exhibiting a pycnocline, 78% reported ~~DMCs~~ C<sub>MD</sub> above the ~~bottom mixed layer depth~~ base of the pycnocline (BMLD). ~~This suggests that the~~ with an average distance equal to  $2.74 \pm 5.21$  m. BMLD ~~is~~ appeared as a vertical boundary ~~trapping up to which~~ subsurface Chl-a ~~maxima~~ distribute in shallow waters ( $\leq 120$  m). ~~BMLD constantly described Chl-a vertical distribution despite surface mixing indicators (depth  $\leq 115$  m)~~, suggesting a significant contribution of deep mixing processes in supporting subsurface production under specific conditions (e.g. ~~prolonged stratification, tidal eyelets, and bathymetry~~). ~~Using~~ Here, ~~we describe and advise~~ BMLD ~~for defining subsurface Chl-a could be as~~ a valuable tool for understanding the spatiotemporal variability of Chl-a in shelf seas, ~~representing and provide a method, and a potential variable for ecological assessments~~ function, to extrapolate it from density profiles.

## Keywords

~~Climate change~~, BMLD, ~~DMC~~ C<sub>MD</sub>, deep mixing, MLD, pycnocline, SCML, shelf sea

ha formattato: Rimando commento, Tipo di carattere: +Corpo (Calibri)

## 1. Introduction

As we begin to manage our oceans and coastal seas for more complex simultaneous uses, such as renewable energy developments, fishing and marine protected areas, it is becoming increasingly important understanding details of primary productivity at fine spatial scales. The temporal and sub-mesoscale (1 to 100 km) spatial patchiness of resources in coastal seas (Goebel et al., 2014; Martin, 2003) indicates a complex interplay of localized factors—such as circulation, river plumes, mixing and stratification—that seasonally characterize the different hydrodynamic regimes of the marine environment (Leeuwen et al., 2015; Cullen, 2015; Lévy et al., 2015). Besides very shallow waters, the vast majority of phytoplankton generally grows in stratified waters, where the pycnocline acts as a barrier against the mixing of the whole water column. The balance between stratification and mixing is determinant for phytoplankton flourishing in the euphotic zone, which, in shelf seas, fluctuates in time and space by the modulation of daily and biweekly tidal cycles (Klymak et al., 2008). Turbulent mixing of the water column requires energy sources from either the surface (e.g. wind stress, Ekman pump due to wind curl) or the deep waters (e.g. upwelling, eddy diffusion, tidal currents). Climate change is introducing variations in these physical factors, and therefore changes are expected in the overall mixing budget of our seas. Anomalies in circulation slow down, sea level rise, bottom and surface temperature have largely been described as driven by climate change in the last two decades (e.g. Bryden et al., 2005; Taboada and Anadón, 2012). However, their effects on the biological effects, especially those from the bottom-up regulation of primary production, are still partially understood (Lozier et al., 2011; Somavilla et al., 2017).

### 1.1 Subsurface chlorophyll-a maxima layers (SCMLs)

As we begin to manage our oceans and shelf seas for more complex simultaneous uses, such as renewable energy developments, fishing and marine protected areas, it is becoming increasingly important understanding details of primary productivity at fine spatial scales. Besides very shallow waters, the vast majority of phytoplankton in continental shelf waters generally grows under stratified conditions, where the pycnocline acts as a barrier against the mixing of the whole water column and allows cells to buoyance and photosynthesize within the euphotic zone. The balance between stratification and mixing in the water column is determinant for phytoplankton, and, in the North Sea, it fluctuates in time and space by the modulation of daily and biweekly strong tidal cycles (Klymak et al., 2008). Turbulent mixing of the water column requires energy sources from either the surface (e.g. wind stress, Ekman pump due to wind curl) or deep waters (e.g. upwelling, eddy diffusion, tidal currents), which can be altered by climate change and man-made infrastructures (Dorrell et al., 2022). Therefore, changes are expected in the overall mixing budget of our seas. Anomalies as circulation slow-down, sea-level rise, bottom and surface temperature, wind speed and wave height have largely been described as a consequence of climate change in the last two decades (e.g. Orihuela-Pinto et al., 2022; Taboada and Anadón, 2012; Bonaduce et al., 2019), while the consequences of these changes on the biological processes are still partially understood (Lozier et al., 2011; Somavilla et al., 2017).

### 1.1 Subsurface chlorophyll-a maxima layers (SCMLs)

Many of the uncertainties of climate change regarding the impacts on primary production come from the difficulties in sampling the community composition and the total abundance throughout the whole water column. ~~The vertical distribution of phytoplankton is one of the most relevant and challenging variables to sample in the marine environment.~~ Contrary to the detection of surface blooms by satellite sensors, subsurface chlorophyll-a maxima layers (SCMLs) are often more difficult to describe and measure. SCMLs represent significant features in plankton systems (Cullen, 2015), they define where most of the bottom-up processes take place and can encompass more than 50% of the entire water

70 column production (Weston et al., 2005; Takahashi and Hori, 1984). In the North Sea, the summertime (May-August) subsurface production contributes to the annual production of up to 20-50% and sustain the food chain in continental shelf waters during prolonged stratified conditions (Hickman et al., 2012; Richardson and Pedersen, 1998; Weston et al., 2005). Several studies linked the vertical distribution of maximum chlorophyll-a (Chl-a) to deep mixing processes (e.g. Brown et al., 2015; Richardson and Pedersen, 1998; Sharples et al., 2006; Zhao et al., 2019b)(e.g. Brown et al., 2015; Richardson and Pedersen, 1998; Sharples et al., 2006; Zhao et al., 2019b) and identified the occurrence of deep Chl-a assemblages in the proximity of the pycnocline in shelf seas (e.g. Costa et al., 2020; Durán-Campos et al., 2019; Ross and Sharples, 2007; Sharples et al., 2001)(e.g. Costa et al., 2020; Durán-Campos et al., 2019; Ross and Sharples, 2007; Sharples et al., 2001). Deep turbulent processes and stratification are notably linked in shelf seas, where the stratification is maintained by tidal cycles mixing the water column through horizontal circulation. The stratification is generally controlled by a balance between mixing processes (tidal mixing and surface wind stress) and sources of buoyancy (surface heating and estuarine inputs of low salinity), whose balance allow primary producers to grow in favourable light and nutrient conditions within the pycnocline. In the North Sea, mixing processes are mostly regulated by strong tidal currents (Glorioso and Simpson, 1994; Loder et al., 1992; Sharples et al., 2006, 2001; Simpson et al., 1980; Zhao et al., 2019b)(Glorioso and Simpson, 1994; Loder et al., 1992; Sharples et al., 2006, 2001; Simpson et al., 1980; Zhao et al., 2019b), especially in prolonged stratified conditions, when upward fluxes represent the only source of nutrients intake within the pycnocline. Maxima Chl-a have been identified at the base of the pycnocline in regions of strong tidal mixing at Georges Bank in August (Holligan et al., 1984) and within the western English Channel (Sharples et al., 2001)(Sharples et al., 2001). However, despite the clear linkage between SCMLs and stratified waters, the effects of climate change on tidal mixing in shelf seas, variations on ocean productivity have been mainly been described in relation to conducted at oceanic sites by investigating the mixing processes above the pycnocline (within the upper mixed layer) (Somavilla et al., 2017), omitting the effects of deeper layer processes. In fact, studies of shelf waters suggest fast (Somavilla et al., 2017; Steinacher et al., 2010), omitting the effects of processes close to the seabed, e.g. variations of mixing processes below the pycnocline. On the other hand, studies on shelf waters suggest variations of the water column due to both surface and deep mixing processes, since the interplay of marine components occur within a thinner layer from surface to seabed are more adjacent than in deep oceanic locations (Durski et al., 2004). The exclusive investigation of the surface mixed layer is likely to bias the investigation of climate change impacts on primary production (abundance and distribution) in shallow sea/shelf regions and needs to be investigated further.(Durski et al., 2004).

## 1.2 Mixed layer depth (MLD) and pycnocline characteristics

100 MLD has been largely considered as a central variable for understanding phytoplankton dynamics (Sverdrup, 1953), especially in oceanic sites, where several studies have investigated the ecological relevance of MLD on Chl-a vertical distribution (Behrenfeld, 2010; Carranza et al., 2018; Diehl, 2002; Diehl et al., 2002; Gradone et al., 2020), phytoplankton bloom events (Behrenfeld, 2010; Chiswell, 2011; D'Ortenzio et al., 2014; Prend et al., 2019; Ryan-Keogh and Thomalla, 2020, Sverdrup, 1953), and the effects of climate change (Somavilla et al., 2017). The nutricline exhibits positive correlations with the upper mixed layer depth (Ducklow et al., 2007; Gradone et al., 2020; Holligan et al., 1984; Prézelin et al., 2000, 2004; Ryan-Keogh and Thomalla, 2020; Yentsch, 1974, 1980), and it has been generally associated with surface spring blooms or windstorm events (e.g. Banse, 1987; Carranza et al., 2018; Carvalho et al., 2017; Lande and Wood, 1987; Theriault et al., 1978). However, the effect of climate change on MLD and primary production is still an unsolved question (Lozier et al., 2011; Somavilla et al., 2017). The need for a much more detailed understanding of the linkage between primary production, pycnocline characteristics and deeper turbulent processes (Behrenfeld, 2010; Carranza et al., 2018; Diehl, 2002; Diehl et al., 2002; Gradone et al., 2020), phytoplankton bloom events (Behrenfeld,

ha formattato: Inglese (Regno Unito)

2010; Chiswell, 2011; D'Ortenzio et al., 2014; Prend et al., 2019; Ryan-Keogh and Thomalla, 2020, Sverdrup, 1953), and the effects of climate change (Somavilla et al., 2017). The nutricline's depth exhibits positive correlations with the upper mixed layer depth (Ducklow et al., 2007; Gradone et al., 2020; Holligan et al., 1984; Prézelin et al., 2000, 2004; Ryan-Keogh and Thomalla, 2020; Yentsch, 1974, 1980), and it has been generally associated with surface spring blooms or windstorm events (e.g. Banse, 1987; Carranza et al., 2018; Carvalho et al., 2017; Lande and Wood, 1987; Therriault et al., 1978). However, the effect of climate change on MLD and primary production is still an unsolved question (Lozier et al., 2011; Somavilla et al., 2017). The need for a much more detailed understanding of the linkage between primary production, pycnocline characteristics and deep turbulent processes (below the pycnocline) is therefore a key area of research, especially in highly productive but spatially heterogeneous areas such as shelf waters and shallow seas.

The methods for identifying MLDs vary among marine environments, hydrodynamic regimes, or the spatial resolution of vertical profiles (Courtois et al., 2017; Lorbacher et al., 2006)(Courtois et al., 2017; Lorbacher et al., 2006), because making use of a single method is difficult for spatiotemporally heterogeneous regions. MLDs are typically defined as the depth at which the density gradient exceeds a specific value (threshold) (e.g. Kara et al., 2000), however this method presents issues in specific hydrodynamic conditions, such as over estimating MLD in regions with deep convection (e.g. subpolar oceans) (Courtois et al., 2017), or misidentifying water columns with a newly established shallow MLD over previous periods of stratification (Somavilla et al., 2017)(Somavilla et al., 2017). Several sensitivity tests and comparisons have been conducted in oceanic waters (e.g. Carvalho et al., 2017; Courtois et al., 2017; González-Pola et al., 2007; Holte and Talley, 2009), however, there are no standard methods of investigation that adapts MLD's for MLD identification neither in shelf nor oceanic waters.

### 1.3 A new way forward: the base of the pycnocline (BMLD) as an ecological indicator of the vertical distribution of maximum proxy for Chl-a (DMC) maximum in shelf waters

In this study, we proposed the adaptation of existing methods into a new algorithm able to cope with different high-resolution (1 m) vertical distributions of the density (therefore being able to deal with split pycnoclines and unusual shapes) to characterize the heterogeneity of coastal/shelf/shallow waters and identify the depth between the pycnocline and i) the surface mixed layer depth (commonly known as "MLD", here renamed as above mixed layer depth, AMLD) and ii) the bottom below mixed layer depth (BMLD). The method is validated for a region in waters depths from 20 to 120 m, with 14 years of repeated surveys that covers a mosaic of habitats types in waters depths ranging from 20 to 120 m (north-western North Sea) driven by seasonal stratification stratified waters, permanently mixed waters, regions of freshwater inputs and strong tidal mixing (Leeuwen et al., 2015). We investigated the ecological relevance of both layers (AMLD and BMLD) in relation to the vertical distribution and abundance of Chl-a, and we compared the performance of these two proposed density layers to some of the other methods used in the literature. This new level of understanding (Leeuwen et al., 2015). The vertical distribution of density and Chl-a profiles are compared and the biological relevance of BMLD in investigating subsurface Chl-a is detailed. This approach is being developed in order to help the identification of key linkages between the physical environment and primary production at finer spatial scales (punctual location up to  $\leq 1$  km), which can be ecologically relevant for pressing issues in marine spatial management (e.g. seabed leasing for wind farms, locations of MPAs) and spatially explicit climate change assessments.

## 2. Methods

Vertical samples of density and Chl-a (see Sect. 2.1) were used to characterize the relationship between stratification features (see Sect. 2.2 and 2.3) and subsurface Chl-a (described as abundance and vertical distribution, see Sect. 2.2) and

ha formattato: Tipo di carattere: Non Corsivo

150 stratification features (see Sect. 2.3 and 2.4) in shelf waters < 120 m (2.4). The most frequent methods used to identify  
vertical characteristics of density profiles (density layers/levels – DLs) (see Sect. 2.3) were compared to the proposed  
algorithm estimating the above and below limits of the pycnocline (AMLD and BMLD in Fig. 2). This algorithm is able  
to cope with density profiles having instability, or the pycnocline fractured in sections (see, Sect. 2.2-4). Here, a new  
method identifying to identify BMLD is proposed, and its ecological application (together with other six DLs) potential  
155 is evaluated by comparing it with the vertical distribution of subsurface Chl-a during spring and summer (April-August)  
(see Sect. 2.5).

## 2.1 Physical and biological oceanographic samples

160 *In situ* summertime measurements of temperature, salinity, and fluorescence (Chlorophyll-a proxy of Chl-a abundance)  
were collected from a towed, undulating, CTD and a vertical CTD in the North Sea off the East coast of Scotland, UK,  
within the Firth of Forth (FoF) and Tay region for over 14 years (from 2000 to 2014) (Fig. 1). A total of 1273 profiles  
from both types of sampling were extracted from April to August (April=3, May=51, June=1115, July=66, August=38).  
426 profiles were gathered using the vertical CTD from 12 oceanographic campaigns carried out by Marine Scotland  
Science on board of the fisheries research vessels *Scotia* and *Alba na Mara* (www.gov.scot/marine-and-fisheries). The  
data set comprises temperature, conductivity, and fluorescence/Chl-a measurements from the sea surface to the seabed  
165 (vertical resolution equals to 1 decibar) at a number of fixed stations sites from 2000 to 2014. Water samples were  
collected during each cast for calibration of the *in situ* sensor data. Temperature and conductivity measurements were  
quality controlled using the standard Marine Scotland Science editing procedure. The undulating CTD sampled the water  
column in June 2003 and July 2014 with a continuous vertical and horizontal oscillation of the instrument throughout the  
water column from 2 to 5 m below the sea surface to 5 m from the seabed. The continuous profiles obtained from  
170 undulating CTD were converted into 847 single profiles of the water columns. Data were sampled at 1 second intervals,  
resulting in a vertical resolution comprising between 0.5 and 1 m, in water depths from 25 m to 115 m. More information  
about the oceanographic cruise in June 2003 are described in Scott et al. (2010), and the same method was used in July  
2014. The processing of undulating CTD enabled to get 847 single profiles of the water columns. Overall, 1273 profiles  
from both types of sampling were extracted from April to August (April=3, May=51, June=1115, July=66, August=38).  
175 *In situ* conductivity were converted first in Practical Salinity ( $S_p$ ), then into Absolute Salinity ( $S_A$ ), and *in situ* temperature  
was converted into Conservative temperature ( $\Theta$ ) to calculate density ( $\rho$ ) (*gsw\_rho* function), using the TEOS-10  
toolboxes (www.teos-10.org) within the *gsw* v1.0.5 package in R v3.6.3 (R Core Team, 2018) (2010), whose method was  
used also in July 2014.

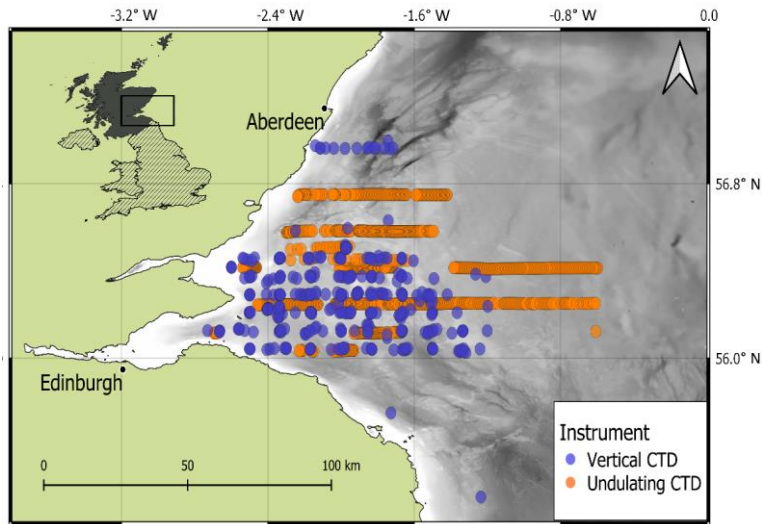
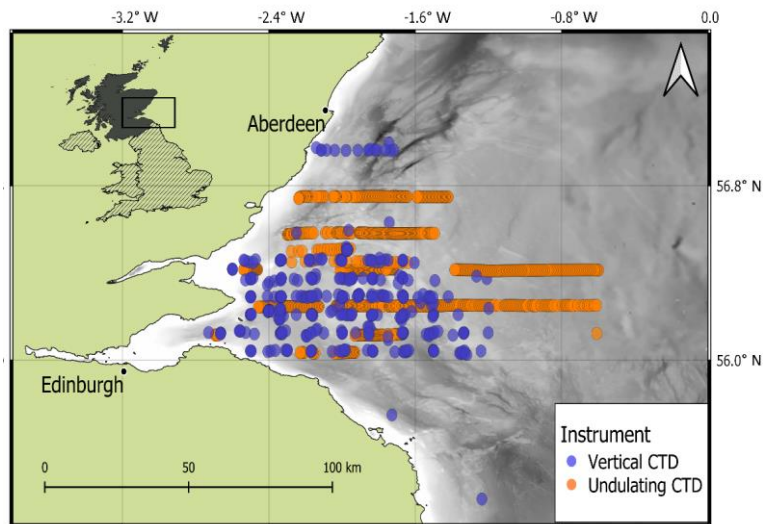


Figure 1: Study area with the in situ surveys measured by an undulating CTD (orange dots) and a vertical CTD (blue dots). Land (green) and bathymetry (grey colour ramp) are pictured (ESRI 2020; EMODnet 2018)

### 2.1.1 Standardized vertical sampling for density and Chl-a profiles

Since the proposed algorithm (described in Sect. 2.32) works with profiles at high vertical resolution (samples' distance vertical resolution is 1 m), the in situ casts were required to be standardized throughout the water column. Density ( $\rho$ ) and Chl-a observations taken every 0.5 to 1 m from undulating CTD were converted into measurements over regular depth intervals by smoothing and interpolating. This was achieved by fitting a generalized additive model (GAM) (Hastie and Tibshirani, 1990) using an adaptive spline with  $\rho$ -or-Chl-a, as a function of depth. The smoothing basis (knots) were selected in a range from 75% to 90% of the number of observations occurring within each profile. The obtained smooth function for each profile was used to predict/interpolate  $\rho$ -and-Chl-a at regular 1 m depth intervals. In order to maintain the same shape and values in each profile, the fitted curves at 1 m interval were visually checked by plotting the estimated and real profiles to visually identify possible errors. 154.16% of the shapes ( $n=8953$ ) were manually corrected by changing the number of knots in the GAM. The pre-processing analysis resulted in advantageously eliminating multiple sampling at the same depth that would have affected the selection of density layers' depths and maxima Chl-a, especially in transects with undulating CTD. Appendix A. The analyses were run in R v3.6.3 (R Core Team, 2018) using the *mgcv* v1.8-33 package.

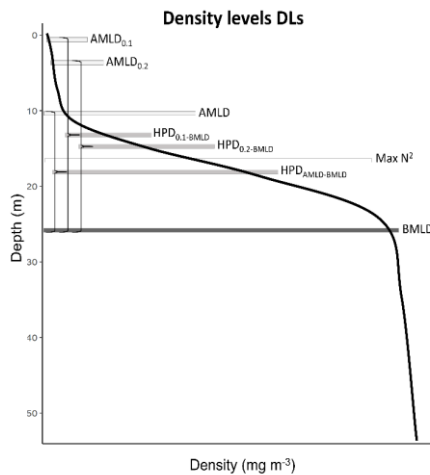


## 2.2 AMLD and BMLD detection

### 200 *Definition of AMLD and BMLD*

205 In stratified waters, the layers above and below the pycnocline are mixed vertical region where the density gradient is significantly different from the pycnocline. The surface mixed layer depth (AMLD) and the mixed layer depth below the pycnocline (BMLD) are both transitional layers from a mixed to a stratified vertical region occurring at the beginning and end of the pycnocline. The most common threshold methods (see Sect 2.3) identify AMLD based on the principle that the mixed layer at the surface has a density's variance close to zero, which separates from the pycnocline, exhibiting a larger density gradient. The above assumptions may not always hold, especially when the upper mixed layer is heterogeneous with nested sub-structures such as small re-stratification at the surface, or when the pycnocline can include a small mixed layer (Fig. A1a, e, f in Appendix A) or presents different density gradients (stratified layers) within it (Fig. A1b and c in Appendix A). Such density conditions are difficult to isolate with the available methods.

210 In the proposed algorithm, the detection of AMLD does not assume that the mixed layer has a density gradient close to zero, and it identifies MLDs regardless any *a priori* threshold. It also picks up the shallowest and deepest limits of the pycnocline by excluding middle breaks of the pycnocline, allowing the identification for unconventional density vertical distribution. The definition of AMLD and BMLD are based on common conventions: small and similar  $\Delta\rho$  (measured as the difference between two consecutive points,  $\Delta\rho_z = |\rho_z - \rho_{z+1}|$ ) within the mixed layers and within the pycnocline; the pycnocline is enclosed by layers of mixed water above and/or below it exhibiting a different  $\Delta\rho$ ; the mixed layer depth is pinpointed independently from a fixed gradient (Chu and Fan, 2019, 2011; Holte and Talley, 2009). The AMLD represents the last depths up to which  $\Delta\rho$  is consistently small from the surface to the pycnocline, while the BMLD is the first depth after the pycnocline from which  $\Delta\rho$  is consistently small up to the seabed (Fig. 2).



220 Figure 2: The eight density levels (DLs) are reported for a generic density profile. The curly brackets define the halfway depths (HPDs) between AMLD's indicators (AMLD<sub>0.1</sub>, AMLD<sub>0.2</sub>, AMLD) and BMLD.

Method to extract AMLD and BMLD

225 AMLD and BMLD have been identified developing an algorithm based on Chu and Fan (2011) framework to produce a method able to cope with various density profiles exhibiting a pycnocline (examples in Fig. A1 in Appendix A). The algorithm's sequence identifies the depth with the largest density difference between a mixed and a stratified layer using i) an adaptation of the maximum angle method (Chu and Fan, 2011) and ii) a cluster analysis on the density difference at each observed depth ( $\Delta\rho_z = |\rho_z - \rho_{z+1}|$ ). The method is designed to work with equal, high-resolution, intervals of density values ( $z$ ) in the profiles. In order to distinguish AMLD from BMLD, their selection is achieved by splitting the number of observations throughout the profile into two distinct groups, *Split1* and *Split2* (Fig. 3), each one respectively

230 used to identify AMLD and BMLD. *Split1* includes the density values from the surface ( $z_1$ ) to two measurement intervals ( $\delta$ , here 1 m) above BMLD ( $z_{BMLD} - 2\delta$ ); *Split2* extends from  $2\delta$  above the halfway depth in  $\rho$  range ( $0.5\Delta\rho = ((\rho_{max} - \rho_{min})/2) - 2$ ) to the ninetieth portion of the profile from the surface to the seabed ( $z_{0.9\Delta\rho} = 90\%$  of  $z$ ) (Fig. 3). For all depths between  $z_1$  and  $z_{0.9\Delta\rho}$ , the angle  $\varphi$  has been measured at  $z(x, y)$  (where  $x$  and  $y$  are density and depth) between two vectors ( $V1, V2$ ) fitting a linear regression ( $y \sim x$ ). Although Chu and Fan (2011) suggested to measure the tangent of the angle between  $V1$  and  $V2$  ( $\varphi$ ), we encountered some issues identifying BMLD in those profiles where density decreases below the pycnocline (Fig. A1d, Appendix A) and  $\varphi$  is bigger than 90 degrees. However, the exclusive use of the maximum angle method would have biased the selection due to local variation and instability conditions of the water column (Fig. A1b, c, e, f in Appendix A). Therefore, a K-Mean cluster analysis (Lloyd, 1982) was adopted in the algorithm to improve the selection of the pycnocline limits by classifying the density difference at depth ( $\Delta\rho_z = |\rho_z - \rho_{z+1}|$ ) into groups. The use of K-mean meets the assumption that  $\Delta\rho_z$  values within a mixed layer would belong to a unique cluster. Adding the conditions controlling for a similar classification of  $\Delta\rho_z$  at depths above AMLD and below BMLD resulted in decisive outcomes, correctly identifying the mixed layers within those density profiles having a pycnocline fractured in chunks with different or similar gradients. The algorithm was developed in R v3.6.3 (R Core Team, 2018) and it is

ha formattato: Motivo: Trasparente (Bianco)

ha formattato: Motivo: Trasparente

ha formattato: Motivo: Trasparente (Bianco)

available as a function (*abmdl.R*) to download from GitHub (<https://github.com/azampollo/BMLD>). A more detailed description of the method is also reported in Supplementary Materials at the GitHub page.

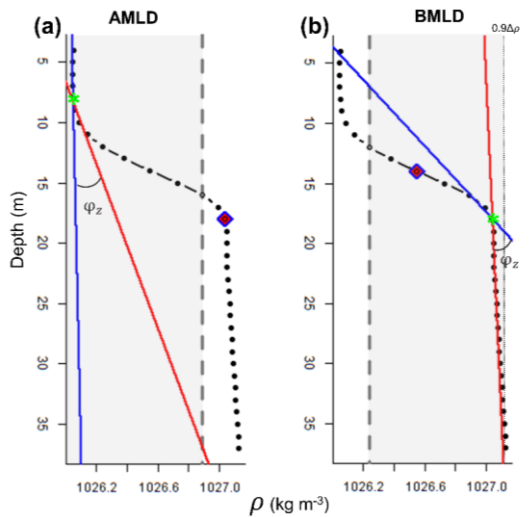


Figure 3: plots of a density profile reporting the attributes calculated by the algorithm: grey region includes the observations (black dots) used to identify AMLD and BMLD, which extends in (a) from the surface to  $2\delta$  before BMLD (purple rhombus), and in (b) from  $2\delta$  before the reference point ( $0.5\Delta\rho$ , purple rhombus) to  $0.9\Delta\rho$ . The solid blue and red lines refer to the vectors V1 and V2 reporting the angle  $\varphi_z$  used to identify AMLD and BMLD (green stars).

#### Performance of the algorithm

Following the assumptions described above, the algorithm failed to correctly identify AMLD and BMLD and classified the two limits of the pycnocline within it (examples in Fig. A1, Appendix A). The selection was considered to have failed when the AMLD and BMLD were selected  $\geq 2$  m (2 observations) above or below the mixed layer depth. Major errors in identifying AMLD (6.76% of the profiles) and BMLD (4.32%) occurred in density profiles with a high number of observations in the portion of the water column where mixed layer was transitioning into the pycnocline, where  $\varphi_z$  was similar amongst several observations and the cluster analysis was identifying observations at the end of the pycnocline as part of the mixed layer (e.g. Fig. A1 a-c, Appendix A). It is important to highlight the sensitivity of this method to  $\Delta\rho$  at AMLD and BMLD (a large  $\Delta\rho$  is preferred), and the sampling frequency at the transition between the pycnocline and the above and below mixed layers. The algorithm did not correctly identify AMLD in profiles without a surface mixed layer, and a shallow pycnocline that comprised two different gradients (Fig. A1c, Appendix A). In this case, the cluster analysis split  $\Delta\rho$  into two groups, although they belong to the same pycnocline. Other errors were related to profiles having a pycnocline split into two parts by a thin mixed layer with height  $> 4$  m (4 observations) (Fig. A1e, Appendix A). Overall, the identification of BMLD performed better than AMLD's, although it could not deal with profiles having less than 4 observations throughout the pycnocline (in this study thickness of the pycnocline  $< 3$  m). This condition occurred due to the location of the *Split2* (which is necessary to distinguish BMLD's from AMLD's selection) i) at depths above AMLD (misidentifying AMLD as BMLD) or ii) too close to BMLD (missing enough observations to fit properly V1). The

algorithm always correctly selected BMLD in profiles that have a lower density observation below the BMLD (Fig. A1d, Appendix A).

### 2.3 Common methods identifying Density Levels (DLs)

Among the methods used to detect density levels in coastal and oceanic waters, three approaches were selected to define mixing and buoyancy features in the sampled profiles.

The AMLDs are typically defined as MLD in the literature and represent the depth at which the density exceeds a specific value (threshold method) (e.g. Kara et al., 2000). The threshold is typically selected among a range of values previously tested in the literature (from 0.0025 to 0.125 kg m<sup>-3</sup>) (summarized in Thomson and Fine, 2003; Montégut et al., 2004; Lorbacher et al., 2006; Holte and Talley, 2009) and measured as the difference ( $\Delta\rho_z = |\rho_z - \rho_{ref}|$ ), between a certain sampling depth ( $z$ ) and a reference density value ( $\rho_{ref}$ ), which can be the density at the surface, at 10 m depth, or a consecutive point (e.g.  $z-1$ ). In this study, two density thresholds (0.01 and 0.02 kg m<sup>-3</sup>) have been measured as the difference between two consecutive points in the profile ( $\Delta\rho_z = |\rho_z - \rho_{z+1}|$ ) and named as AMLD<sub>0.01</sub> and AMLD<sub>0.02</sub>. Since previous studies identified subsurface Chl-a in the proximity of the centre of the pycnocline (here called halfway pycnocline depth, HPD, Table 1), we investigated the relationship between Cmd (depth of maximum Chl-a) and three different HPDs measured as the halfway depth between the base of the pycnocline (BMLD) and AMLD<sub>0.01</sub>, AMLD<sub>0.02</sub> and adjusted AMLD, and named HPD<sub>0.01-BMLD</sub>, HPD<sub>0.02-BMLD</sub>, and HPD<sub>AML-BMLD</sub> (Fig. 2).

Moreover, several studies reported positive correlation between the maximum squared buoyancy frequency (Max N<sup>2</sup>) and Cmd at oceanic sites (e.g. Martin et al., 2010; Schofield et al., 2015; Carvalho et al., 2017; Courtois et al., 2017; Baetge et al., 2020) and shelf waters (Lips et al., 2010; Zhang et al., 2016). Therefore, the depth of Max N<sup>2</sup> has been selected from N<sup>2</sup> profiles computed by *gsw.Nsquared* function (*gsw* v1.0-5 package) in R v3.6.3 (R Core Team, 2018), following the most recent version of the Gibbs equation of state for seawater in TEOS-10 systems (Intergovernmental Oceanographic Commission, 2010). The magnitude of N<sup>2</sup> quantifies the stability of the water column and pinpoints the stratified layers where the energy required to exchange water parcels in the vertical direction is maximum (Boehrer and Schultze, 2009).

Table 1: Table of abbreviations used in the paper.

Abbreviation	Description
SCML	Subsurface Chlorophyll-a maximum Layer
Chl-a	Chlorophyll-a (mg m <sup>-3</sup> )
Cmd	Depth of maximum Chlorophyll-a (m)
DL	General abbreviation for a density layer (e.g. AMLD, BMLD, HPD, or Max N <sup>2</sup> ) (m)
MLD	General expression for Mixed layer depth (m)
AML	Above mixed layer depth, or starting point of the pycnocline (m)
BML	Below mixed layer depth, or ending point of the pycnocline (m)
HPD	Halfway pycnocline depth, or centre of the pycnocline (m)
Max N <sup>2</sup>	maximum squared buoyancy frequency (N <sup>2</sup> ) (m)

### 2.4 Subsurface Chlorophyll-a parameters

ha formattato: Tipo di carattere: +Corpo (Calibri)

*The depth of maximum Chl-a (DMC) Figure 1: Study area with the in situ surveys measured by an undulating CTD (orange dots) and a vertical CTD (blue dots). Land (green) and bathymetry (grey colour ramp) are pictured (ESRI 2020; EMODnet 2018)*

### 2.21.1 Subsurface Chlorophyll a parameters

The depth of maximum Chl-a (DMC) was defined as the deepest maximum inflection point in the Chl-a profile standardized at 1 m sampling frequency (Carvalho et al., 2017; Zhao et al., 2019b), by using the adapted Chu and Fan (2011) method to measure described in Sect 2.2. The DMC was selected throughout each vertical profile of Chl-a as the real depth having the maximum angle instead of the tangent of  $(\varphi)$  (Eq. (1)) between two vectors ( $V_1$  and see details in Sect. 2.4);  $V_2$ ). Details on the number of observations used to fit each vector are reported in Supplementary materials. The automated identification of DMC was checked manually with a visual inspection of each profile. The total amount of Chl-a were measured using trapezoidal integration (Walsby, 1997) throughout the water column (depth-integrated Chl-a) in R v3.6.3 (R Core Team, 2018).

The vertical distribution of Chl-a was classified into six most frequent vertical shapes according to the literature (Lavigne et al., 2015; Mignot et al., 2011; Uitz et al., 2006; Zhao et al., 2019a), using terminology adopted from Mignot et al., 2011 and Zhao et al., 2019. The profile was split in two sublayers, one above and one below the depth of maximum Chl-a (DMC), upper and lower sublayers (Fig. 2a grey solid line), and three equal sections were used to divide the difference between the minimum and maximum Chl-a values into three equal sections (Fig. 2a red dashed lines). The identification of the shapes was performed visually with the help of an automatic measuring of the ratio of observations in the three vertical sections within the upper and lower sublayers (Fig. 2). The few profiles with unclear subdivisions, or very different shapes, were excluded from the dataset (which only represented 2% of the data).

First, the gaussian shapes, which were not determined by the ratio of observations within each section, have been pulled from the dataset and gathered into two shapes, the "Narrow-SCM" and "Wide-SCM", since the profiles exhibited two main widths of standard deviations of Chl-a from DMC. The Narrow-SCM shape is defined by the decrease of Chl-a from DMC within a limited range of depths (3-10 m) (Fig. 2a), while Wide-SCM shape is characterized by the equal decrease of Chl-a within a wide range of depths above and below DMC, whose gaussian curvature often covers the whole water column (Fig. 2b). The "SCM-HCU" shape exhibits a high ratio of Chl-a in the first lower and second upper sections (Fig. 2c), while the "SCM-HCL" shape is characterized by a high ratio in the first upper and second lower sections (Fig. 2d). The "HCL" and "HCU" shapes are defined by the section with the highest ratio of Chl-a in the lower sublayer: HCL is characterized by most of the observations within the third section (Fig. 2e), while the HCU exhibits a high number of observations within the first section (Fig. 2f).

ha formattato: Motivo: Trasparente (Bianco)

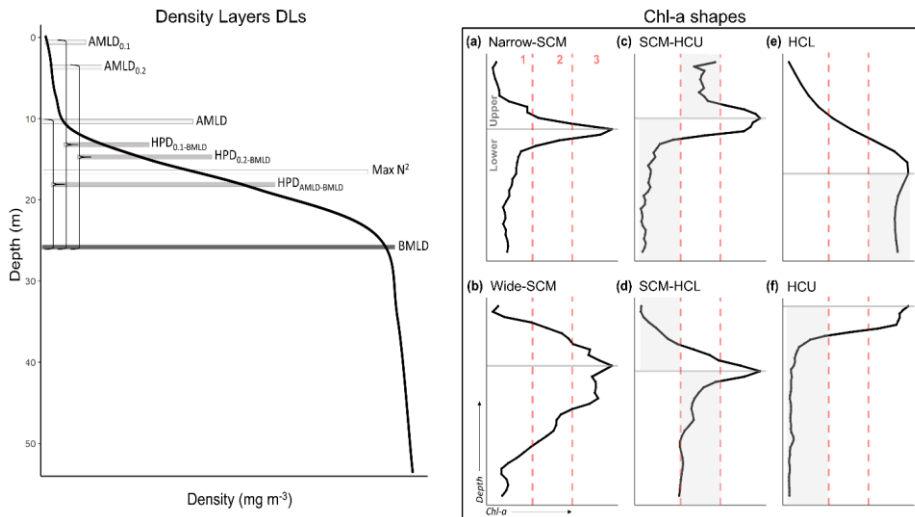


Figure 2: The eight density layers (DLs) are reported for a generic density profile (on the left, together with an example for each of the six (plots a-f) identified Chl-a shapes (on the right). On the density profile, the curly brackets define the halfway depth (HPD) between AMLD's indicators ( $AML D_{0.1}$ ,  $AML D_{0.2}$ ,  $AML D$ ) and BMLD. The Chl-a shapes are split into the upper and lower sublayers at the DMC (horizontal solid grey line) (a). The vertical lines indicate the limits of sections 1, 2 and 3 (dashed red lines) (a) that were used to identify the type of shape. The grey shaded squares represent the sections with the highest ratio of Chl-a determining SCM-HCU and SCM-HCL, HCL and HCU.

Table 1: Table with the abbreviations used in the paper.

Abbreviation	Description
SCML	Subsurface-Chlorophyll-a maximum Layer
Chl-a	Chlorophyll-a ( $mg\ m^{-3}$ )
DMC	Depth of maximum-Chlorophyll-a (m)
DL	General abbreviation for a density layer (e.g. AMLD, BMLD, HPD, or $Max\ N^2$ ) (m)
MLD	General expression for Mixed layer depth (m)
AML D	Above mixed layer depth, or starting point of the pycnocline (m)
BML D	Below mixed layer depth, or ending point of the pycnocline (m)
HPD	Halfway pycnocline depth, or centre of the pycnocline (m)
$Max\ N^2$	Maximum water buoyancy frequency ( $N^2$ ) (m)

### 2.3 Common methods identifying Density Layers (DLs)

among the methods used to detect density layers in coastal and oceanic waters, three approaches were selected to define mixing and buoyancy features in the sampled profiles.

The AMLDs are typically defined as MLD in the literature and represent the depth at which the density gradient exceeds a specific value (threshold method) (e.g. Kara et al., 2000). The threshold is typically selected among a range of values previously tested in the literature (from 0.0025 to 0.125 kg m<sup>-3</sup>) (summarized in Holte and Talley, 2009; Lorbacher et al., 2006; Montégut et al., 2004) and measured as the difference ( $\Delta\rho_z = |\rho_z - \rho_{zz}|$ ) between a certain sampling depth ( $z$ ) and a reference density value ( $\rho_{zz}$ ), which can be the density at the surface, 10-m depth, or a consecutive point (e.g.  $z+1$ ). In this study, two density gradients (0.01 and 0.02 kg m<sup>-3</sup>) have been measured as the difference between two consecutive points in the profile ( $\Delta\rho_z = |\rho_z - \rho_{z+1}|$ ) and named as AMLD<sub>0.01</sub> and AMLD<sub>0.02</sub>.

Since previous studies identified DMCs in the proximity of the centre of the pycnocline (HPD), we investigated the relationship between DMCs and three different HPDs measured as the halfway depth between the base of the pycnocline (BMLD, see Sect. 2.4) and AMLD<sub>0.01</sub>, AMLD<sub>0.02</sub> and adjusted AMLD (the last described in Sect. 2.4), and named HPD<sub>0.01-BMLD</sub>, HPD<sub>0.02-BMLD</sub>, and HPD<sub>AMLD-BMLD</sub> (Fig. 2).

Moreover, the association of maximum buoyancy frequency squared (Max N<sup>2</sup>) with DMC and Chl-*a* abundance has been investigated since several studies reported positive correlation at oceanic (e.g. Martin et al., 2010; Schofield et al., 2015; Carvalho et al., 2017; Courtois et al., 2017; Baetge et al., 2020) and shelf waters (Lips et al., 2010; Zhang et al., 2016). For each profile, the depth of Max N<sup>2</sup> has been selected from N<sup>2</sup> profiles (Fig. 2) computed by *gsw\_Nsquared* function (*gsw* v1.0.5 package) in R v3.6.3 (R Core Team, 2018), which is based on absolute salinity and conservative temperature with respect to pressure following the most recent version of the Gibbs equation of state for seawater in TEOS-10 systems (Intergovernmental Oceanographic Commission, 2010). The magnitude of N<sup>2</sup> quantifies the stability of the water column and pinpoints the stratified layers where the energy required to exchange water parcels in the vertical direction is maximum (Boehrer and Schultze, 2009).

#### 2.4.1 AMLD and BMLD detection

Theoretically, the layers between the pycnocline and a mixed vertical region above and below the pycnocline are depths showing a large change in the density gradient. The surface mixed layer depth (AMLD) and the mixed layer depth below the pycnocline (BMLD) are both transient layers from a mixed to a stratified vertical region occurring at the beginning and end of the pycnocline. The threshold methods (see Sect. 2.3) delineate an AMLD's identification based on the principle that the mixed layer at the surface is characterized by a variance of  $\Delta\rho$  close to zero. They assume that the pycnocline is the portion of the water column with a large density gradient  $\Delta\rho$  that separates two portions of mixed waters (above and below it) exhibiting a low and similar  $\Delta\rho$ . These assumptions may not always hold, and we found that identification failure can occur when the upper mixed layer is heterogeneous, with nested sub-structures such as small re-stratification at the surface followed by a small mixed layer before the pycnocline (Fig. A1e in Appendix A), or when the pycnocline is fractured in chunks (Fig. A1f in Appendix A). These conditions are difficult to isolate using the maximum angle (Chu and Fan, 2011) and threshold methods. In this paper, the AMLD's definition does not assume that the surface mixed layer is fully mixed with a  $\Delta\rho$  close to zero for the whole portion of the water column, and it identifies AMLD regardless any *a priori* threshold. It also picks up the shallowest and deepest limits of the pycnocline by excluding middle breaks of the pycnocline, allowing the identification of unconventional density vertical distribution. Instead, here, the definition of AMLD and BMLD are based on common conventions: small and similar variations in the density gradient within the mixed layer, above and below the pycnocline; the pycnocline is enclosed by mixed portions of the water column above and/or below it exhibiting a significant variation of the density gradient; the depth with the largest density is pinpointed independently from a fixed gradient (Chu and Fan, 2019, 2011; Holte and Talley, 2009).

ha formattato: Tipo di carattere: +Corpo (Calibri)

380 AMLD and BMLD have been identified developing an algorithm based on Chu and Fan (2011) framework to produce a method able to cope with various density profiles exhibiting a pycnocline (examples in Fig. A1 in Appendix A). The algorithm's sequence identifies the depth with the largest density gradient between a mixed and a stratified layer using i) an adaptation of the maximum angle method (Chu and Fan, 2011) and ii) a cluster analysis on the density gradient ( $\Delta\rho_z = |\rho_z - \rho_{z+1}|$ ) (diagram of the algorithm in Fig. 3a). The method is designed to work with equal, high-resolution, intervals of density values ( $z$ ) in the profiles. In order to distinguish AMLD from BMLD, their selection is achieved by splitting the observations throughout the profile into two distinct groups, *Split1* and *Split2* (Fig. 3b and Fig. 3c), each one respectively used to identify AMLD and BMLD. *Split1* includes the density values within the first observation close to the surface ( $z_s$ ) and two measurement intervals  $\delta$  (here 1 m) above BMLD ( $z_{\text{BMLD}} - 2\delta$ ), while *Split2* extends from  $2\delta$  above the depth halfway through the  $\rho$  range ( $0.5\Delta\rho = ((\rho_{\text{max}} - \rho_{\text{min}})/2) - 2$ ) up to the depth at which the total number of points from the surface to the bottom amounts up to 90% of the entire profile ( $z_{0.9\Delta\rho} = 90\%$  of  $\frac{\rho}{z}$ ). Since *Split1* is based on BMLD, the algorithm identifies AMLD after BMLD.

390 For all depths between  $z_s$  and  $z_{0.9\Delta\rho}$ , the angle  $\varphi$  has been measured at  $z(x, y)$  (where  $x$  is the density and  $y$  is depth) between two vectors ( $V1, V2$ ) fitting a linear regression ( $y \sim x$ ) each. The two vectors have been calculated using  $2\delta$  before and after each observation ( $z$ ) ( $V1 =$  from  $[z - 2]$  to  $z$ , and  $V2 =$  from  $z$  to  $[z + 2]$ ) (Fig. 3b and Fig. 3c). Although Chu and Fan (2011) suggested to measure the tangent of the angle between  $V1$  and  $V2$  ( $\varphi$ ), we encountered some issues identifying BMLD in those profiles that decreased in density below the BMLD (Fig. A1d, Appendix A). Therefore, the algorithm has been improved by calculating the angle  $\varphi$ . Since the slope (or angular coefficient,  $\beta$ ) of a linear regression is the tangent of the angle between the line and the  $x$ -axis, the angle  $\varphi$  was obtained from two angles extracted from the coefficients measured by  $V1$  and  $V2$  according to the sign of  $\beta$ : i) positive  $\beta$  (see example in Fig. 3d, angle  $\tau$  and the orange vector) refers to the angle between the vector and the horizontal plane with  $y$  equal to the intercept ( $\alpha$ ), or ii) negative  $\beta$  (see example in Fig. 3d, angle  $\omega$  and the blue vector) refers to the angle between the vector and the vertical plane with  $x = 0$ . The angle  $\varphi$  at each observation ( $\varphi_z$ ) is measured by summing up, or subtracting, the angles derived from the coefficients,  $\beta_x$  and  $\beta_z$  for  $V1$  and  $V2$ , according to their partial contribution to  $\varphi$ , which can be summarized under four different conditions:

$$400 \varphi_z = \begin{cases} \text{atan}(|\beta_x|) + \text{atan}(|\beta_z|), & \beta_x > 0 \text{ and } \beta_z > 0 \\ \text{atan}(|\beta_x|) - \left(\frac{\pi}{2} - \text{atan}(|\beta_z|)\right), & \beta_x > 0 \text{ and } \beta_z < 0 \\ \text{atan}(|\beta_x|) + \left(\frac{\pi}{2} - \text{atan}(|\beta_z|)\right), & \beta_x < 0 \text{ and } \beta_z > 0 \\ |\text{atan}(|\beta_x|) - \text{atan}(|\beta_z|)|, & \beta_x < 0 \text{ and } \beta_z < 0 \end{cases} \quad (1)$$

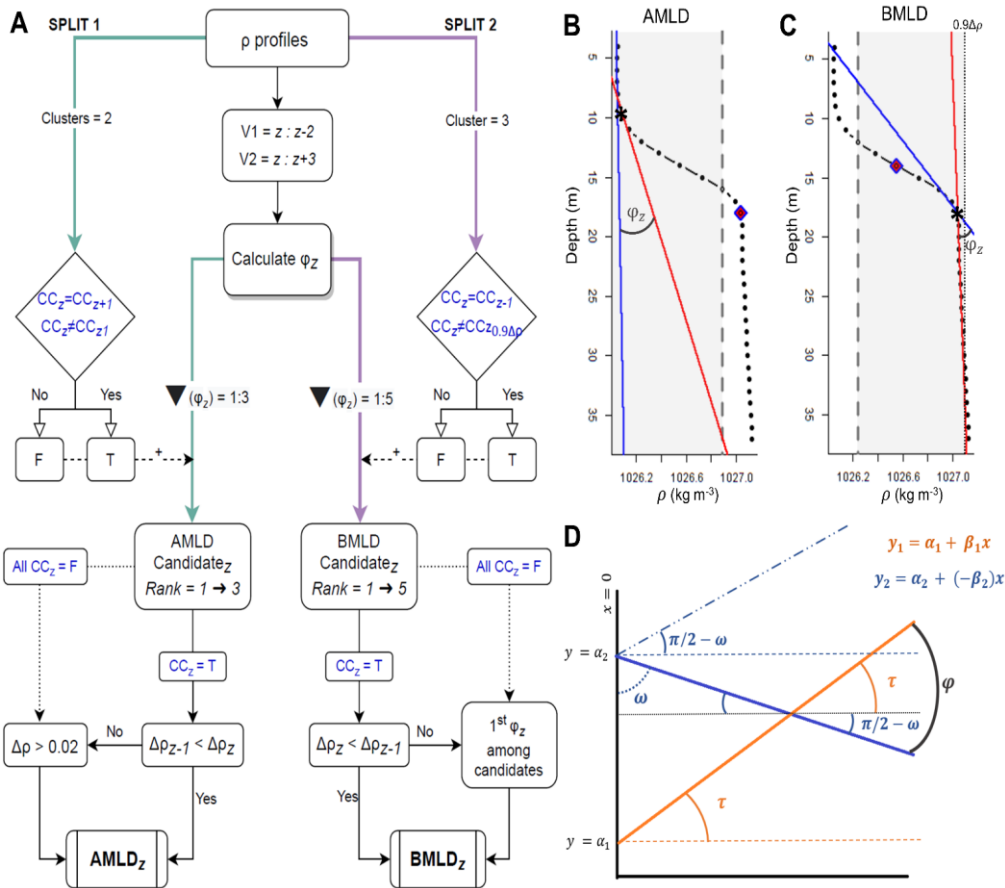
where  $\text{atan}()$  refers to the arctangent of the coefficients  $\beta_x$  and  $\beta_z$ .

405 Up to this stage, the algorithm selects AMLD and BMLD on the adapted maximum angle method (Chu and Fan, 2011). However, the exclusive use of the maximum angle method would have biased the selection due to local variation and instability conditions of the water column (Fig. A1b, c, e, f in Appendix A). Therefore, a K-Mean cluster analysis (Lloyd, 1982) was adopted in the algorithm to improve the selection of the pycnocline limits by adding a further step of selection on the 3 and 5 largest  $\varphi$  for AMLD and BMLD, respectively. Since the transition from surface mixing layer to the pycnocline is sharper than that one from the pycnocline to the bottom mixing layer, the number of  $\varphi$  candidates is higher in BMLD than in AMLD selections. The cluster analysis classifies the density gradient at depth ( $\Delta\rho_z = |\rho_z - \rho_{z+1}|$ ) into groups (see below), assuming that  $\Delta\rho_z$  values within a mixed layer would belong to a unique cluster.

ha formattato: Motivo: Trasparente

415 AMLD's selection is made amongst the 3 largest  $\varphi$ , and the first  $\varphi_z$  amongst the descendent ordered candidates meeting the following conditions was assigned as AMLD: i) the observations ( $z$ ) within the mixed water column belong to the same cluster classification (CC), the candidate  $\varphi_z$  must have  $CC_z = CC_{z+1}$  and  $CC_z \neq CC_{z+1}$  (CC at surface  $z+1$ ), ii) and  $\Delta\rho_{z-1} < \Delta\rho_z$ . In AMLD's selection, the  $\Delta\rho_z$  is grouped in two clusters since we would expect two main variations of  $\Delta\rho$  in *Split1*: a small gradient on the surface mixed section and a bigger one at the pycnocline due to stratification. The same approach has been adopted for BMLD's identification amongst the 5 largest  $\varphi$ , although the inclusion of three clusters instead of two improved the performance of the algorithm since the region of the water column transiting from the pycnocline to the bottom mixed layer is smoother than in AMLDs (e.g. Fig. A1b in Appendix A).  
420 The first  $\varphi_z$  amongst the descendent ordered candidates meeting the following conditions was selected as BMLD: i)  $CC_z = CC_{z+1}$  and  $CC_z \neq CC_{z+0.9\Delta\rho}$  (CC at the  $z=0.9\Delta\rho$ ), and ii)  $\Delta\rho_z < \Delta\rho_{z-1}$ . Adding the conditions controlling for a similar classification of  $\Delta\rho_z$  at depths above AMLD and below BMLD resulted in decisive outcomes, correctly identifying the mixed layers within those density profiles having a pycnocline fractured in chunks with different or similar gradients. However, when the conditions associated with clustering were not found among the candidates  $\varphi$ , the algorithm was not necessary and therefore the simplest methods were adopted to select i) AMLD with a threshold gradient  $\Delta\rho_z > 0.02 \text{ mg m}^{-2}$ , and ii) BMLD as the largest  $\varphi$  (Fig. 3a). The algorithm was developed in R v3.6.3 (R Core Team, 2018), and the K-mean density was calculated using the *kmeans* function using Lloyd (1982) algorithm (*stats* package).  
425

ha formattato: Motivo: Trasparente (Bianco)



430 *Figure 3: main steps of AMLD and BMLD selection: (a) diagram of the algorithms, where green arrows belongs to*  
*Split1 and purple arrows to Split2, text in blue is the portion of the algorithm relying on cluster analysis (K-mean), “F”*  
*and “T” are the results, false and true, of the conditions expressed in the rhombuses. The  $\varphi$  is measured for each*  
*observation ( $z$ ), and the largest (3 for AMLD and 5 for BMLD)  $\varphi$  are considered as candidates of AMLD and BMLD.*  
*The candidates are descendent ordered (Rank 1 → 3 or Rank 1 → 5) and the first candidate meeting the other*  
435 *conditions will be identified as AMLD or BMLD. If any candidate meets the conditions, the original methods are used*  
*(threshold method  $> 0.02$  and maximum angle  $\varphi$ ). (b) and (c) are plots of the same density profile representing the*  
*attributes used in the algorithm: grey region includes the observations (black dots) used to identify AMLD and BMLD,*  
*which extends in (b) from the surface to two depths above BMLD (purple rhombus), and in (c) from two depths above*  
440 *the middle of the pycnocline (purple rhombus) to  $0.9\Delta\rho$ . AMLD and BMLD are reported by a black star in (b) and (c)*  
*respectively. In (b) and (c), the vectors V1 (blue line) and V2 (red line) are drawn for each  $z$  (black star) and  $\varphi_z$  is*  
*reported. Plot (d) shows of one of the four conditions reported in Eq. (1) measuring  $\varphi$ : V1 (orange line) with a positive*  
*slope ( $\beta_x$ ) and V2 (blue line) with a negative slope ( $\beta_x$ ).*

## 2.5 Evaluating the association between density layers and levels with subsurface Chl-a

The ecological relevance of each density layer level (DL) was evaluated by comparing their coincidence with the depth of maximum Chl-a (DMCCMd) (e.g. DMCCMd = BMLD) and the predictability of DMC (y) from each DL (x); their strength in predicting CMd. The coincidence and the prediction of DMCCMs from a density characteristic are profiles return important tools for understanding of the processes driving subsurface concentrations and identifying identify a valuable proxy for modelling analyses and for controlling uncertainty in net primary production estimates.

In this study, we evaluated the coincidence of the DMCCMd with eight investigated density layers levels (AMLD<sub>0.01</sub>, AMLD<sub>0.02</sub>, AMLD, BMLD, HPD<sub>0.01-BMLD</sub>, HPD<sub>0.02-BMLD</sub>, HPD<sub>AMLD-BMLD</sub>, and Max N<sup>2</sup>, Fig. 2, described in Sect. 2.3 and 2.42) using Spearman's rank correlation coefficient ( $\rho_s$ ) and a Major Axis (MA) line fitting, and the prediction of DMCCMd from DL by performing a linear regression model (LM). The Spearman's coefficient (Eq. (21) in Table 2) assesses a monotonic linear relationship with values ranging between -1 and +1, which refer to a perfect negative or positive correlation between two variables. Besides the strength of the linear relationship defined by  $\rho_s$ , we focused on evaluating the linear relationship between DMCCMd and each DL using 3 different linear models  $y = \alpha + \beta x$ : 1) alpha and beta estimated by linear regression (Eq. (4) in Table 2); 2) alpha and beta estimated by major axis line fitting; and 3) the one-to-one line linear regression with alpha and beta fixed at 0 and 1 respectively (Eq. (4) in Table 2). The one-to-one line hypothesizes that CMd and DL occur at the same depth. The MA is largely used to investigate how one variable scales against another by accounting for errors from both directions (x and y) and measuring the residuals perpendicular to the line (details in the review Warton et al., 2006). Therefore, the aim of MA is not to predict the y-variable, however evaluating the proximity of the coefficients of the estimated MA line ( $\alpha$  and  $\beta$ ) to the scenario in which DL equals DMCCMd. The coincidence of each DL and DMCCMd was summarized by reporting the  $\alpha$  and  $\beta$  MA coefficients, which are here hypothesized to reflect the one-to-one line (be intercept  $\sim 0$ , and slope  $\sim 1$ ) if when CMd occurs at the DMC is aligned with same depth of the DL in question.

Since the identification of a proxy for subsurface Chl-a represents a useful tool for correctly assessing the abundance and the variations of primary production, we investigated the power of prediction of DMCCMd from each DL by measuring the r-squared ( $R^2$ ) from i) an ordinary least square to estimate parameters from the observations in a linear regression (Eq. (32) in Table 2), and ii) the one-to-one linear regression (which has been forced with the intercept through the origin and a slope equal to 1, Eq. (43) in Table 2). The formulae used to calculate the coefficient of determination  $R^2$  for the one-to-one ( $R_0^2$ ) and empirical ( $R_{em}^2$ ) LMs have been summarized in Eq. (32) and Eq. (4)-(3) in Table 2).

Table 2: Formulae for estimating the bivariate line-fitting, Spearman's rank correlation coefficient ( $\rho_s$ ), coefficient of determination  $R^2$  for testing the one-to-one linear regression ( $R_0^2$ ) (e.g. DMCCMd  $\sim$  BMLD) and the empirical linear regression ( $R_{em}^2$ ).

	Formula	Purpose
$\rho_s$	$\frac{\sigma_{xy}}{\sigma_x \sigma_y} \quad (21)$	Estimate the strength of the relationship between x and y
$R_{em}^2$	$1 - \frac{SS_{RES}}{SS_{TOT}} = 1 - \frac{\sum_{i=1}^n (y_i - \hat{y}_i)^2}{\sum_{i=1}^n (y_i - \bar{y})^2} \quad (32)$	Measure the variation in y that is explained by x in a LM
$R_0^2$	$1 - \frac{SS_{RES}}{SS_{TOT}} = 1 - \frac{\sum_{i=1}^n (y_i - x_i)^2}{\sum_{i=1}^n (y_i)^2} \quad (43)$	Measure the variation in y that is explained by x in a one-to-one LM

475 Notation:  $\sigma_{xy}$  is the covariance of  $x$  and  $y$ ,  $\sigma_x$  and  $\sigma_y$  are standard deviations,  $n$  is the number of observations of  $x$  and  
480  $y$ ,  $y_i$  is  $DMC_i$ ,  $\bar{y}$  is the average of  $DMCs$ , and  $x_i$  is the density layers related to  $DMCCMd$  in each regression (e.g.  
 $DMCCMd \sim BMLD$ ).  $SS_{RES}$  is the residual sum of squares,  $SS_{TOT}$  is the total sum of squares.

In the empirical LM,  $R_{em}^2$  was calculated using the typical formula with the residual sum of squares ( $SS_{RES}$ ) as the square  
of the difference of  $y$  and  $\hat{y}$  (estimated  $y$  from the model) (Eq. (3) in Table 2). In the one-to-one LM, the  $SS_{RES}$  in  
480  $R_0^2$  was adapted by replacing  $\hat{y}$  with  $x$  (Eq. (4) in Table 2), (3), since the values of  $x$  and  $y$  are assumed to be equal in the  
one-to-one line regression and the difference between them should be zero. The two  $R^2$  differ also for the denominator  
 $SS_{TOT}$ , which is the sum of squares about the average of the explanatory variable in  $R_{em}^2$  and the sum of squares of the  
 $DMCCMd$  values since in  $R_0^2$  the value of  $DMCCMd$  and DL equals.

Since the  $SS_{TOT}$  adopted in the two formulae is different, the proportion of explained  $DMCs$ ' variance by each DL  
485 can be compared only within each linear regression rather than across the one-to-one and empirical regressions. Therefore,  
the power of prediction among DLs was discussed in within each type of LM.

### 3. Results

The presented algorithm identifying for AMLD and BMLD was applied to the 1273 profiles exhibiting a pycnocline (see  
Sect. 3.1), whose The associations with  $DMCs$  (and without the other density layers—levels (AMLD<sub>0.01</sub>, AMLD<sub>0.02</sub>,  
490 AMLD, HPD<sub>0.01-BMLD</sub>, HPD<sub>0.02-BMLD</sub>, HPD<sub>AMLD-BMLD</sub>, BMLD and Max N<sup>2</sup>) are described for the whole dataset (see Sect.  
3.2) and for each Chl- $a$  with  $CMds$  and the vertical distribution (see of Chl- $a$  are described in Sect. 3.1 and 3). 2.

#### 3.1 Identification of AMLD and BMLD density levels

The above mixed layer depth (AMLD) and the below mixed layer depth (BMLD) were identified by merging existing  
methods into an algorithm able to process density profiles with a 1 m sampling resolution. The algorithm was applied to  
495 the 1273 profiles exhibiting a pycnocline with heterogeneous vertical distributions, e.g. having a small re-stratification at  
the surface followed by a mixed layer before the pycnocline, or a pycnocline fractured in sections (examples of density  
profiles in Fig. A1, Appendix A).

Here, the identifications of AMLD and BMLD did not assume that the mixed layer has a density gradient ( $\Delta\rho$ ) close to  
zero (e.g. threshold methods). Instead, the occurrence of a layer (the pycnocline) having  $\Delta\rho$  at any observation  $z$  ( $\Delta\rho_z =$   
500  $|\rho_z - \rho_{z+1}|$ ) pointedly Chl- $a$  maximum (CMd) was compared to eight different from that within the above and below  
(mixed) layers, is assumed. Therefore, the algorithm pinpoints the transition from the mixed layers to the pycnocline  
based on similar variations in  $\Delta\rho$  within the mixed layer and within the pycnocline. As Fig. 2 shows, the algorithm was  
created to identify i) AMLD as the depth between a surface mixed layer having  $\Delta\rho$  similar among observations and a  
layer (pycnocline) exhibiting an increasing  $\Delta\rho_z$  after AMLD, and ii) BMLD as the depth at which  $\Delta\rho_z$  is smaller than at  
505 the pycnocline and consistently similar among observations up to the seabed. This identification does not consider the  
pycnocline as a layer with a constant  $\Delta\rho$  throughout its whole extension, since the pycnocline can include a small mixed  
layer (Fig. A1a, c, f in Appendix A) or presents different density gradients (stratified layers) within it (Fig. A1b and e in  
Appendix A). Therefore, the AMLD represents the last depths up to which the  $\Delta\rho$  is consistently small from the surface  
to the pycnocline, while the BMLD is the first depth after a layer with large  $\Delta\rho$  from which the density gradient is  
510 consistently small down to the seabed (or the deepest observation). In the algorithm, the similarity amongst  $\Delta\rho_z$  was  
measured using a cluster analysis (see Sect. 2.4), which defines the main conditions controlling the selection of AMLD  
and BMLD by hypothesising that the mixed layer (up to AMLD or from BMLD) must have density gradients belonging

ha formattato: Non Apice / Pedice

Formattato: Paragrafo elenco

ha formattato: Tipo di carattere: 10 pt

ha formattato: Tipo di carattere: 10 pt

to the same cluster. However, in specific conditions the algorithm failed to correctly identify AMLD and BMLD and classified the two limits of the pycnocline within it (Fig. A1, Appendix A). The selection was considered to have failed when the AMLD and BMLD were selected  $\geq 2$  m (2 observations) above or below the mixed layer depth. Major errors in identifying AMLD (6.76% of the profiles) and BMLD (4.32%) occurred in density profiles with a high number of observations within the transition from the mixed layer to the pycnocline, where  $\sigma_z$  was similar amongst several observations and the cluster analysis was identifying the gradients close to the end of the pycnocline as belonging to the mixed layer (e.g. Fig. A1 a-c, Appendix A). The number of candidates appeared to be sensitive to the sampling frequency and the thickness of the transition regions (AMLD-pycnocline, pycnocline-BMLD). Therefore, it is important to highlight the sensitivity of this method to the rate of change of the gradients at AMLD and BMLD (a large rate of change is preferred), and the sampling frequency at the transition between the pycnocline and the above and below mixed layers. The algorithm did not correctly identify AMLD in profiles without a surface mixed layer, and a shallow pycnoclines that comprised two different gradients (Fig. A1c). In this case, the cluster analysis split  $\Delta\rho$  into two groups, although they belong to the same pycnocline. Other errors were related to profiles having a pycnocline split into two by a small mixed layer within a depth range  $> 4$  m (4 observations) (Fig. A1e). Overall, the identification of BMLD performed better than AMLD's, although it could not deal with profiles having less than 4 observations throughout the pycnocline (in this study thickness of the pycnocline  $< 3$  m). This condition occurred due to the location of the *Split2* (which is necessary to distinguish BMLD's from AMLD's selection) i) at depths above AMLD (misidentifying AMLD as BMLD) or ii) too close to BMLD (missing enough observations to fit properly V1). The algorithm always correctly selected BMLD in profiles that have the lowest densities below the BMLD (Fig. A1d).

### 3.2 DMC association with different characteristic levels of the density profile

The depth of maximum Chl-a (DMC) was compared to the location of eight features of the density profiles (DLs described in Sect. 2.3 and 2.4, Fig. 2) that are summarised in surface mixed layer depth (AMLD<sub>0.01</sub>, AMLD<sub>0.02</sub>, AMLD), bottom below mixed layer depth (BMLD), the centre of the pycnocline (HPD<sub>0.01-BMLD</sub>, HPD<sub>0.02-BMLD</sub>, HPD<sub>AMLD-BMLD</sub>) and the depth of maximum buoyancy frequency squared (Max N<sup>2</sup>) to evaluate i) the strength of a positive linear relationship between each DL and DMC, and ii) the power of prediction of DMC by each DL.

The observations carried out in the FoF and Tay region confirmed the subsurface presence of maxima Chl-a between April and August, with CMDs distributing on average ( $\pm$  standard deviation) at  $19.29 \pm 6.56$  m. All the methods classifying the surface mixed layer (AMLD<sub>0.01</sub>, AMLD<sub>0.02</sub> and AMLD) showed the location of these density layers to be generally shallower than DMCs (Fig. 4 a-c, Table 3) with a rare coincidence of their vertical distribution (from 0.39% to 1.73% of the profiles, Table 3). In particular, the two thresholds' methods used to identify AMLD (0.01 and 0.02 mg m<sup>-3</sup>) exhibited the lowest Spearman correlation amongst all DLs, with AMLD<sub>0.01</sub> having almost a zero correlation to DMCs ( $\rho_s = -0.01$  and 0.08 for AMLD<sub>0.01</sub> and AMLD<sub>0.02</sub>, Table 3) and a null explanation of the DMC's variability in the empirical linear regressions ( $R_{em}^2 = 0.00$  and 0.01, Table 3). The Major Axis analysis identified measured intercepts and slope values in AMLD<sub>0.01</sub> and AMLD<sub>0.02</sub> almost perpendicular to the y-axis due to the strong presence of DMCs in deep waters. Although a clear subsurface aggregation of max-Chl-a maxima occurs below the surface mixed layer (Fig. 4c), the AMLD identified by the algorithm (Sect. 2.4) showed a better correlation with DMC to CMD than AMLD<sub>0.01</sub> and AMLD<sub>0.02</sub>, with a positive linear relationship between the two variables and a greater explained variance of DMC by the one-to-one and empirical linear regressions (Table 3). The coefficients measured by MA for AMLD (Table 3) reported a positive correlation of CMDs, representing a gradual deepening of CMD with the pycnocline.

ha formattato: Tipo di carattere: Non Grassetto

555 Max  $N^2$  is the density layerlevel performing least well after AMLDs in predicting DMCsCMds, although it showed the highest percentage of coincidence with DMCsCMds (13.51% of the profiles, Table 23). Similar to AMLDs, DMCsCMds have been recorded in 64.96% of the profiles at layers deeper than Max  $N^2$ , indicating that max-Chl-a maxima area located in waters below surface mixing, at stratified regions within the pycnocline.

560 Overall, the centre of the pycnocline (HPDs) distributed closeperformed better than AMLD and Max  $N^2$ , distributing closer to DMCs, withCMds. HPD<sub>AML-D-BMLD</sub> exhibiting the highest performance;reported the highest correlation to DMCsCMds ( $\rho_s = 0.56$ ), and the highest explained DMCsCMd's variance from the one-to-one ( $R_0^2 = 0.90$ ) and empirical ( $R_{em}^2 = 0.31$ ) LMslinear regressions (Table 3). The location of DMCsCMds is highly related to HPD<sub>AML-D-BMLD</sub>, although only 4.63% of the profiles presented DMCsCMds and HPD<sub>AML-D-BMLD</sub> at the same depth (Table 3). Many profiles exhibited DMC<sub>CMd</sub> deeper than HPD<sub>AML-D-BMLD</sub> (78.69%), of which 81.53% distributed DMCsCMds above BMLD (hence, between HPD<sub>AML-D-BMLD</sub> and BMLD). HPD<sub>0.01-BMLD</sub>, HPD<sub>0.02-BMLD</sub> less related to CMds in Spearman's correlation, MA, one-to-one and empirical linear regressions than the HPD<sub>AML-D-BMLD</sub> (Table 3).

565 The below mixed layer depth, BMLD, exhibited a reverse condition compared to the other density layerslevels by encompassing 78.32% of DMCsCMds in waters above it (Table 23). BMLDs is the second variable after HPD<sub>AML-D-BMLD</sub> with the highest correlation to DMCsCMds ( $\rho_s = 0.55$ ), it. It is distributed at the same depth of DMCsCMds in 7.86% of the profiles and linearly predicted the location of maxima Chl-a in both one-to-one and empirical linear regressions (Table 23). BMLD exhibited MA coefficients ( $\alpha = 0.60$  and  $\beta = 0.82$ ) close to the hypothesized one-to-one fitting-line ( $\alpha = 0$  and  $\beta = 1$ ), indicating a good approximation of DMCs at BMLD-CMds at the base of the pycnocline. Moreover, CMds distributed on average at  $2.74 \pm 5.21$  m above BMLD, with a maximum distance above it equals to 22 m, and 27 m below it.

575 The overall distribution of DMCsCMds is discernible mainly (> 95.84% of profiles) below the surface mixed layers (AMLDs' indicators), within the deepest half of the pycnocline (between HPD<sub>AML-D-BMLD</sub> and BMLD) and it is bounded for 78.32% of the observations above the BMLD. However, although DMCs, Although CMds generally reflect the region with the highest concentration of Chl-a throughout the water column, the vertical eonecentrationdistribution of phytoplankton-Chl-a can vary in the proximity of DMCsCMds and accumulate mainly above or below it (Fig. 4). The, Hence, the ecological relevance of the density layerslevels has therefore been investigated in comparison with differentthe vertical distribution of Chl-a profile shapes (Fig. 5(Sect. 3.3)).

ha formattato: Pedice

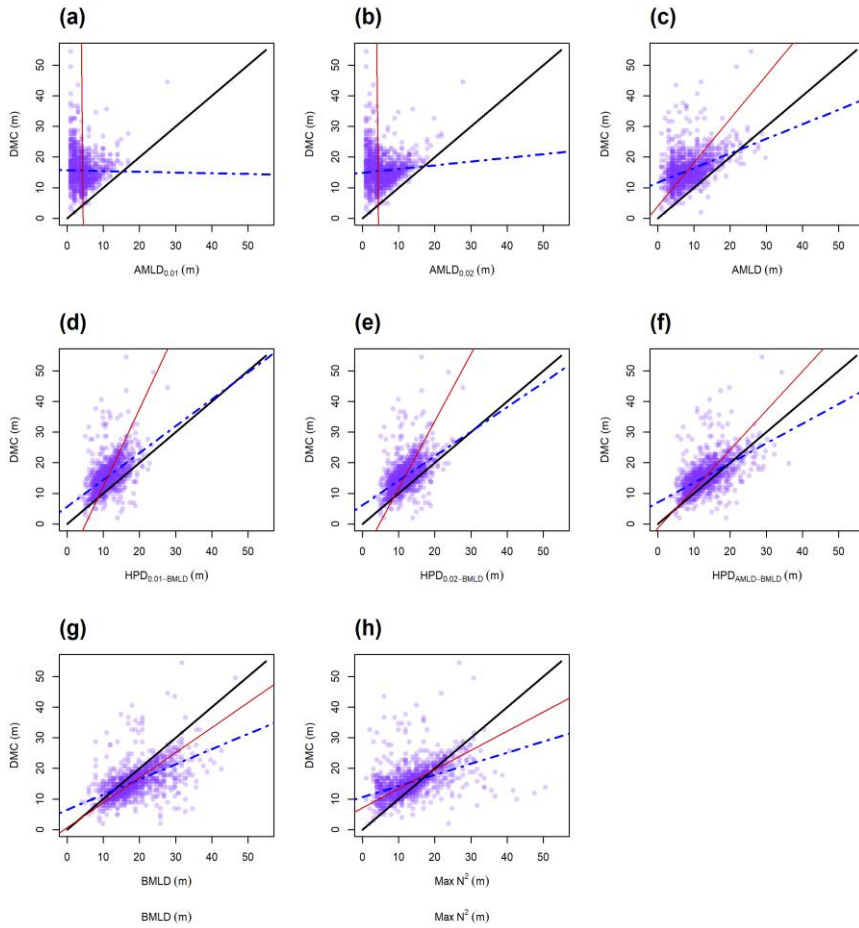


Figure 4-4: Scatterplots of  $\mathcal{DMCCMd}$  and the eight DLs (a-h). The lines refer to the one-to-one linear regression (LM) (solid black), the Major Axis analysis (MA) (solid red), the empirical LM measured from the observations ( $\mathcal{DMCCMd} \sim DL$ ) (dot-dashed blue).

585

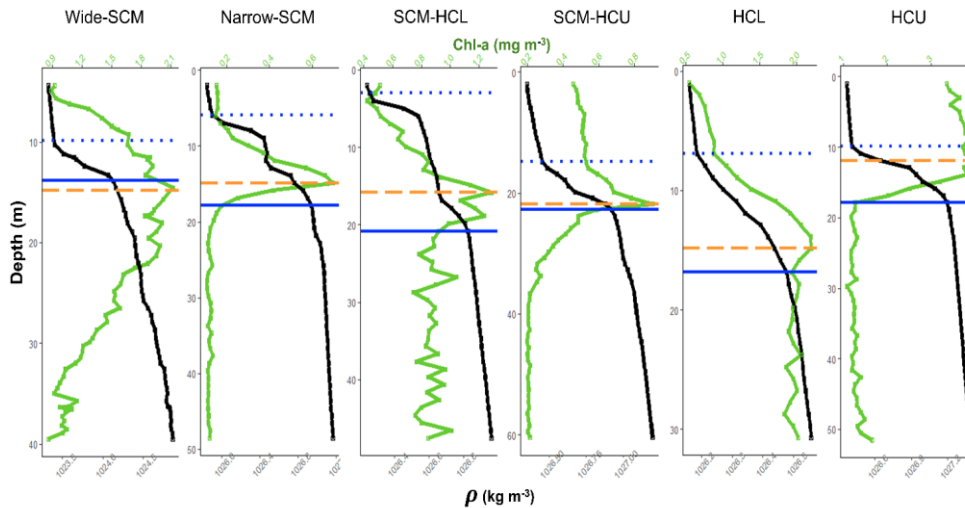
Table 3: Statistical parameters and profiles' percentagespercentage of profiles having  $\mathcal{DMCCMd}$ s above (>), at the same depth (=), or below (<) each DL.

DL	$\rho_s$	$\alpha$	$\beta$	$R_0^2$	$R_{em}^2$	$\mathcal{DMCCMd}$ > DL	$\mathcal{DMCCMd}$ = DL	$\mathcal{DMCCMd}$ < DL
AMLD <sub>0.01</sub>	-0.01	543.35	-124.26	0.40	0.00	99.53	0.39	0.08
AMLD <sub>0.02</sub>	0.08	-43.72	11.35	0.47	0.01	99.45	0.31	0.24
AMLD	0.41	4.01	1.42	0.69	0.17	95.84	1.73	2.44

HPD <sub>0.01-BMLD</sub>	0.52	-12.81	2.52	0.86	0.27	90.18	1.81	8.01
HPD <sub>0.02-BMLD</sub>	0.52	-10.20	2.19	0.87	0.27	86.41	3.77	9.82
HPD <sub>AML-D-BMLD</sub>	0.56	1.31	1.28	0.90	0.31	74.86	4.63	20.50
BMLD	0.55	0.60	0.82	0.87	0.31	13.83	7.86	78.32
Max N <sup>2</sup>	0.45	7.06	0.63	0.84	0.20	64.96	13.51	21.52

### 3.3.3.2 Chl-a vertical distribution in relation to density layers/levels

590 Since hydrodynamic and biological conditions generating resuspension, passive drift, and mortality (i.e. zooplankton grazing in stratified waters) shape Chl-a differently throughout the water column through processes such as resuspension, passive drift, and mortality (i.e. zooplankton grazing in stratified and stable waters), Chl-a can have very different vertically distributions in relation to DMC values (Fig. 5).



595 **Figure 5:** Example, the amount of Chl-a was measured above and below each density levels regardless the vertical distribution of Chl-a (green solid line) and density (black solid line). The horizontal lines indicate BMLD (blue solid), AMLD (blue dotted), and DMC (yellow dashed):CMD.

600 The depth-integrated Chl-a was standardized (“standardized depth-integrated Chl-a”) by the number of 1-m observations above and below four DLs (AML, HPD<sub>AML-D-BMLD</sub>, BMLD and Max N<sup>2</sup>) and values were compared (Table 4). AMLD and HPD<sub>AML-D-BMLD</sub> were selected amongst the density layers indicating levels to represent the surface mixed layer and the centre of pycnoclines due to because of their better correlation to DMCCMD (see Sect. 3.21). The amount of Chl-a (mg) at each meter depth (mg m<sup>-1</sup>) above and below the four density layers/levels is reported in Fig. A2 (Appendix A), Table 4 and Figure 5.

605 Following the results in Sect. 3.2, a large portion of Chl-a was measured at depths below AMLD, HPD<sub>AML-D-BMLD</sub> and Max N<sup>2</sup> (Table 4), where DMCs also occurred. HPD<sub>AML-D-BMLD</sub> and Max N<sup>2</sup> delimit almost three times the amount of Chl-a at depths included from these vertical locations to the seabed as compared to the concentrations at the surface. A reverse

Formattato: Normale, Giustificato

ha formattato: Colore carattere: Evidenziatore 1

610

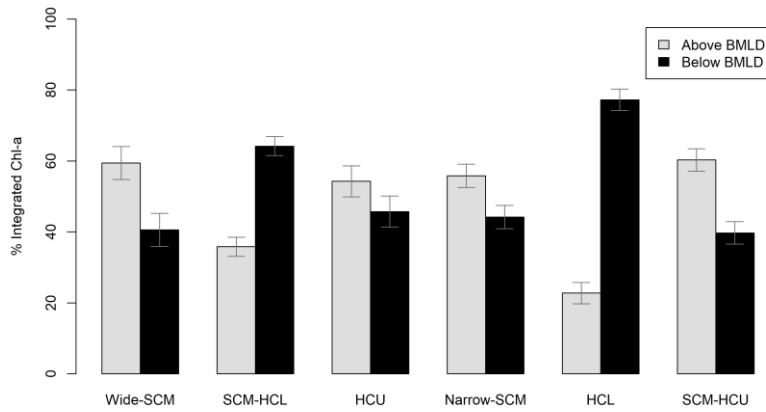
condition is exhibited by Chl-a distributing above and below BMLDs: the standardized depth-integrated Chl-a is higher above than below BMLDs, although the amount of phytoplankton in the deepest layers is still comparable (the difference between surface-BMLD and BMLD-seabed is 42.80 mg m<sup>-1</sup>) (Table 4) (Fig. A2 in Appendix A shows the full distribution of Chl-a values at the 1-m sampling resolution).

615

It is therefore sensible to infer the distribution of DMCs, and the largest portion of phytoplankton at depths enclosed within the stratified region (AMLD—BMLD), to be mainly in the second half of the pycnocline (HPD<sub>AMLD-BMLD</sub>—BMLD). At the same time, a reasonable amount of Chl-a distributes below the pycnocline (BMLD), especially in SCM-HCL and HCL shapes (Fig. 5 and 6).

Table 4: Values of depth-integrated Chl-a (mg) standardized by its range of vertical distribution (m) (Total Chl-a biomass (mg)/depths (m)) above and below the four density layers. These values are also reported in Fig. A2 (Appendix A)-Figure 5.

DL	Standardized depth-integrated Chl-a above DL (mg m <sup>-1</sup> )	Standardized depth-integrated Chl-a below DL (mg m <sup>-1</sup> )
AMLD	172.97	971.12
HPD <sub>AMLD-BMLD</sub>	366.07	859.27
BMLD	615.92	658.72
Max N <sup>2</sup>	372.90	848.14



620

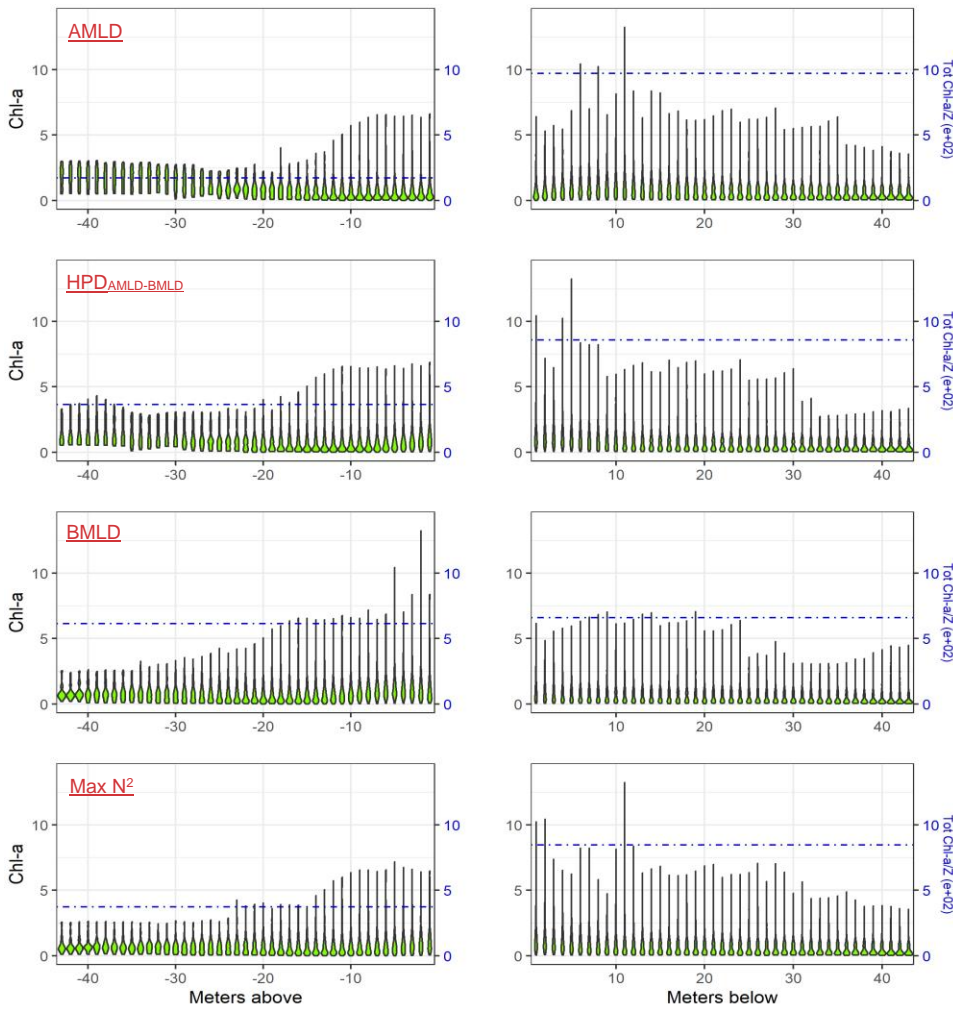


Figure 6- Bar5: Violin plot of the median percentage of Chl-a (mg) at each meter above (light grey) and below (black) BMLD for each Chl-a shape. Grey bars refer to standard error.

### 3.3.1 — DLs associated with Chl-a shapes, with a focus on BMLD

Since BMLD exhibited the clearest pattern in defining the vertical distribution of Chl-a, further investigations have been focused on understanding the relationship between the four density levels (AMLD, HPD<sub>AMLD-BMLD</sub>, BMLD and Chl-a- $\alpha$ -Max N<sup>2</sup>) for the whole dataset. The percentage of dot-dashed blue lines represent the depth-integrated Chl-a measured as the total amount of Chl-a (mg) divided by the number of depths (z) within each portion of the water column (above and below BMLD was measured for each profile and the median-DLs) (values are reported in Fig. 6. HCL and SCM-HCL shapes exhibited a high concentration of Chl-a at depths below BMLD, while SCM-HCU, Narrow-SCM, Wide-SCM and HCU are characterized by large concentrations between the sea surface and BMLD. Table 4).

Formattato: Didascalia, Allineato al centro

ha formattato: Colore carattere: Automatico

635 A distinct pattern of deep Chl-a is visible in HCL shapes, where 77.24% of the total Chl-a was recorded below BMLDs (Fig. 6), and 87.14% of the profiles ( $n=70$ ) reported DMCs in deep mixed waters (Table 5). HCL shape were significantly recorded at shallow bathymetry ( $\leq 63.15$  m) (Wilexon test on bathymetry values at HCL profiles and all the other profiles,  $W = 70534$ ,  $p < 0.00$ ) and exhibited an exceptionally high concentration of Chl-a at DMCs amongst all the other profiles (Wilexon test,  $W = 57303$ ,  $p < 0.00$ ) (Fig. A4b in Appendix A). HCL shapes exhibited a high correlation to BMLD than to the other density layers (Table 5, Tables A1-A7 in Appendix A), although the coincidence of DMC with BMLD occurred only in 1.43% of the profiles. BMLD exhibited a better performance amongst the other density layers in predicting DMCs from both one to one and empirical linear regressions. The MA analysis reported slope values  $< 1$  in all the shapes except HCL, which has the highest  $\beta$  coefficient and the most negative intercept (Fig. 7 and Table 5).

640 The SCM-HCL exhibits, with HCL shape, the greatest linear relationship between DMC and BMLD, showing the highest coincidence of BMLDs and DMCs (10.86% of 405 profiles, Table 5). Amongst all the investigated density layers, DMCs in SCM-HCL locate at depths very close to the base of the pycnocline (Fig. 7 and Table 5) although a large portion of the depth-integrated Chl-a (64.17%) occurred between BMLD and the seabed (Fig. 6). BMLD shows the best performing empirical and one to one linear regressions amongst all the Chl-a shapes (Table 5).

645 The absence of a solid pattern in Wide SCM shape reflects its extensive range of depth at which Chl-a distributes throughout the water column. In Wide-SCM shapes, HPDs' indicators exhibited the highest correlation to DMCs amongst all the density layers (Tables A4-A6 in Appendix A), especially  $HPD_{0.1-BMLD}$  and  $HPD_{0.2-BMLD}$  (Fig. 7) (MA coefficients  $\alpha$  and  $\beta$  close to 0 and 1 respectively), while the percentage of profiles with DMC equal to BMLD appeared higher (7.20%) than HPDs. The one to one and empirical linear regressions similarly report weaker predictability of DMCs from BMLD than the other Chl-a shapes.

650 Since the Narrow-SCM shape typically describes the aggregation of Chl-a within a thin layer of the water column (3-10 m), DMCs are identified between AMLD and BMLD in 83.91% of the profiles ( $n=404$ ), with 55.82% of the total Chl-a between the sea surface and BMLD (Fig. 6). The MA analyses indicate BMLD and  $HPD_{AMLD-BMLD}$  as the closest DLs to DMC amongst all the shapes (Fig. 7), whose  $\alpha$  and  $\beta$  values measured almost 0 and 1 respectively ( $\alpha = 0.26$  and  $\beta = 0.87$  for BMLD,  $\alpha = 0.22$  and  $\beta = 1.13$  for  $HPD_{AMLD-BMLD}$ ). All the DLs except for  $AMLD_{0.01}$  and  $AMLD_{0.02}$  efficiently predicted DMCs from both one to one and empirical linear regressions (Table A1-A7 in Appendix A).

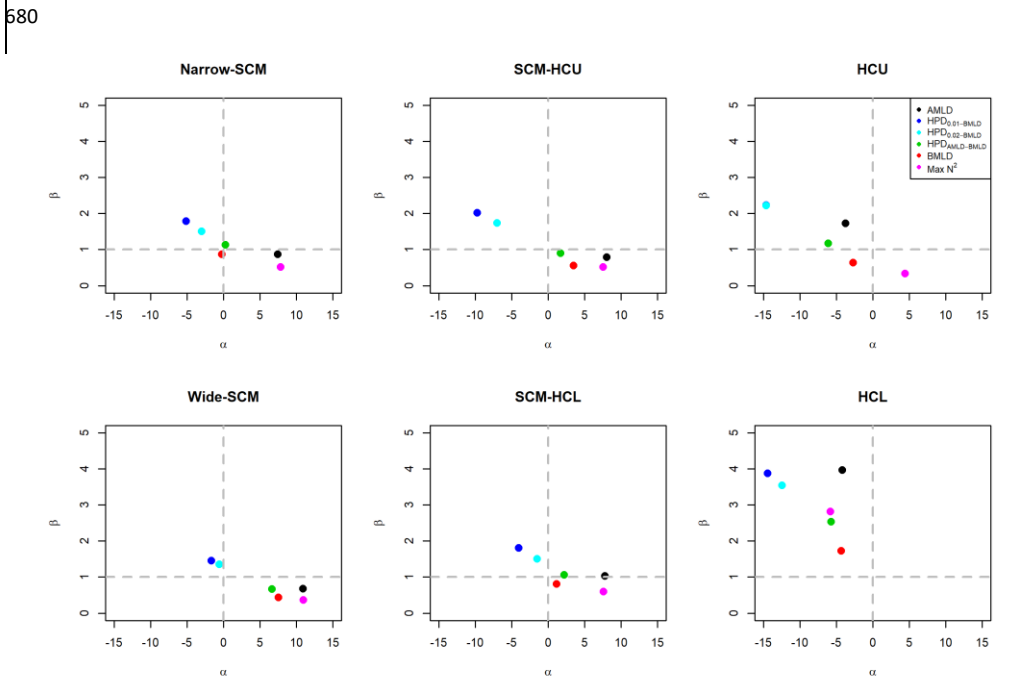
655 The SCM-HCU shape exhibits the highest percentage of depth-integrated Chl-a from the sea surface to BMLD (60.27%, Fig. 6), with 91.02% of the profiles ( $n=245$ ) have the DMC above the base of the pycnocline. The shape showed the highest coincidence of DMCs at  $Max N^2$  (16.88% of the profiles) amongst all the density layers (Tables A7 in Appendix A), although the MA coefficients exhibit a low co-occurrence of DMC at  $Max N^2$  (Fig. 7). The MA analyses indicate BMLD and  $HPD_{AMLD-BMLD}$  as the closest DLs to DMC (Fig. 7); however, the empirical and one to one linear regressions with BMLD and the surface mixing layers performed less well than HPDs' indicators and  $Max N^2$ .

660 For the HCU shapes, the Spearman coefficient shows a low positive correlation between DMCs and DLs, except for the upper mixed layer indicators ( $AMLD$ ,  $AMLD_{0.01}$  and  $AMLD_{0.02}$ ) that occurred at the same depth of DMCs for almost 17% of the profiles ( $n=24$ , Table A1). Following the results in Sect. 3.1, a large portion of Chl-a was measured at depths below AMLD,  $HPD_{AMLD-BMLD}$  and  $Max N^2$  (Table 4), where the depth of Chl-a maximum also occurred. From the seabed to  $HPD_{AMLD-BMLD}$  and  $Max N^2$ , the amount of Chl-a was three times the Chl-a from these DLs to the surface. A reverse condition occurred for Chl-a distributing above and below BMLDs: the standardized depth-integrated Chl-a is higher

670 above BMLDs, although the amount of Chl-a in the deepest layers (below the pycnocline) is still comparable (the  
 difference between Chl-a from the surface to BMLD and from BMLD to seabed is  $42.80 \text{ mg m}^{-1}$ ) (Table 4).

It is therefore sensible to infer the distribution of CMds, and the largest portion of Chl-a at depths enclosed within the  
 stratified region (AMLD – BMLD), especially in the second half of the pycnocline ( $\text{HPD}_{\text{AMLD-BMLD}} - \text{BMLD}$ ). At the  
 same time, a noticeable amount of Chl-a still distributes below the pycnocline (BMLD).

675 **A3 in Appendix A).** Similarly, DMCs occur at the same depth of  $\text{Max N}^2$  for 16.67% of the profiles with a relatively high  
 Spearman coefficient ( $\rho_s = 0.55$ ), although  $\text{Max N}^2$  exhibits the lowest  $R^2_{\beta}$  (0.11) and a low  $\beta$  from the Major Axis  
 analysis ( $\beta = 0.34$ , Table A7 in Appendix A). The same condition refers to BMLD, which predicts only 0.04 of DMC's  
 variance ( $R^2_{\beta}$ ) in HCU shapes and reports DMCs to be always shallower than BMLD (100%, Table 5). Amongst the DLs,  
 BMLD is the density layer with the closest MA coefficients to the ideal co-occurrence of DMCs at BMLD (Fig. 7).



685 *Figure 7: one plot for each Chl-a shape reporting the MA coefficients ( $\alpha$  and  $\beta$ , values reported in Table 5 and Tables  
 A1-A7 in the Appendix A) for six DLs (AMLD<sub>0,1</sub> and AMLD<sub>0,2</sub> were excluded due to their large values visible in Fig. 4 a  
 e). In each plot, the dashed grey lines ( $\alpha=0$  and  $\beta=1$ ) crosses where the DL is hypothesized to occur at the same depth  
 of DMC. Top-right and bottom-left panels (as defined by the dashed grey lines) represent systematic over- and under-  
 estimation respectively, while top-left is under-estimation of the lower values, and bottom-right is over-estimation of the  
 lower values.*

Table 5: Statistical parameters and profiles' percentages having DMCs above (>), at the same depth (=), or below (<) the BMLD.

DL = BMLD									
Chl-a shape	n	$\rho_S$	$\alpha$	$\beta$	$R_g^2$	$R_{cm}^2$	DMC > DL	DMC = DL	DMC < DL
Wide-SCM	125	0.58	7.51	0.44	0.79	0.33	16.00	7.20	76.80
SCM-HCL	405	0.78	1.16	0.81	0.94	0.61	13.33	10.86	75.80
HCU	24	0.55	-2.73	0.65	-0.04	0.30	0.00	0.00	100
Narrow-SCM	404	0.77	-0.26	0.87	0.95	0.59	8.42	7.67	83.91
HCL	70	0.70	-4.36	1.73	0.83	0.49	87.14	1.43	11.43
SCM-HCU	245	0.50	3.48	0.56	0.77	0.25	2.86	6.12	91.02

#### 4. Discussion

In stratified waters, the vertical distribution of Chl-a is partially defined/regulated by physical factors, whose contribution to stabilize the balance of stratification and mixing rate throughout the water column varies across different hydrodynamic regions/regimes over time (Leeuwen et al., 2015). Stratification and mixing characterize the heterogeneous physical environment in shallow and shelf waters. The example here of the North Sea demonstrates the interplay of static (e.g. topography, shelf edge, position of river outflow) and dynamic variables (e.g. wind stress, tidal phases, amount of river outflow, convection or eddy activities), which go on to influence the whole food web at the local scale. (Leeuwen et al., 2015). The combination of static, dynamic and biological factors (e.g. grazing, Benoit-Bird et al., 2013) induces phytoplankton communities to adopt different/adapt their vertical distributions that can be ecologically important/distribution at small scales (< 1 km, Scott et al., 2010; Sharples et al., 2013, < 1 km). Understanding the relationship between Chl-a and vertical density at a fine spatial scale. Identifying a proxy for subsurface concentrations of Chl-a is essential to assess/investigate the effects/impacts of variations in physical processes/changes due to large scale factors (e.g., stratification strength or changes in mixing rate due to wind and tidal renewable energy extraction). In order to identify the vulnerable link of primary production with variations of the hydrodynamic regimes, key physical proxies consistently associated with the different conditions of subsurface Chl-a (shapes) need to be investigated. The differences in the association of DLs, Chl-a shapes and depth-integrated Chl-a with DLs are discussed in the context of previous, sea water increase, or turbulence increase downstream wind turbine foundations). To date several studies in order to understand/have identified the underlying conditions/mixed layer between the sea surface and propose the pycnocline as a valuable tool to help predict subsurface Chl-a at finer scales/assess changes in phytoplankton abundance and phenology over time; here we propose a tool to identify the vertical limits of the pycnocline and indicate the base of the pycnocline (BMLD) as a variable tightly influencing the vertical distribution of Chl-a and likely to affect abundance and phenology.

##### 4.1 Ecological relevance of AMLD and Max N<sup>2</sup> in defining DMCs: valuable in HCU shape CMds.

Oceanic sites exhibit phytoplankton blooms within the upper mixed layer (e.g. Behrenfeld, 2010; Costa et al., 2020; Somavilla et al., 2017) to coincide with AMLDs' vertical fluctuations due to e.g. windstorm events deepening the pycnocline into nutrient-enriched waters (Detoni et al., 2015; Carranza et al., 2018; Höfer et al., 2019; Montes-Hugo et al., 2009). In this study, all the investigated surface mixed layers' indicators (AML<sub>D,0.01</sub>, AML<sub>D,0.02</sub> and AMLD) weakly predicted CMD. The algorithm used in this study has identified AMLD to have an overall higher performance in predicting the location of CMds than the thresholds' methods and maximum squared buoyancy frequency (Max N<sup>2</sup>). Since AMLD

ha formattato: Tipo di carattere: Non Grassetto

720 has been largely considered as a central variable for understanding phytoplankton dynamics (Sverdrup, 1953), it has been investigated in relation to climate change to infer possible significant changes in the amount, spatial distribution and phenology of oceanic primary production (Boyd et al., 2015; Montes-Hugo et al., 2009; Somavilla et al., 2017; Prend et al., 2019; Richardson and Bendtsen, 2019; Schmidt et al., 2020). However, the effect of climate change on AMLD and primary production is still an unsolved question (Lozier et al., 2011; Somavilla et al., 2017). The unclear effects of climate change on AMLD and primary production might be related to i) the type of data used to measure variations in Chl-a, e.g. satellites' observations at the sea surface and their uncertainty related to subsurface Chl-a (Baldry et al., 2020; Erickson et al., 2016; Lee et al., 2015), and ii) the exclusive investigation of the effects of surface mixing processes on primary production (e.g. temperature, wind-induced mixing) by neglecting deep processes that are responsible for the pycnocline's stability (Dave and Lozier, 2015, 2013; Lozier et al., 2011; Somavilla et al., 2017). The AMLD is informative for surface concentrations, but it may not be biologically relevant for subsurface Chl-a that are maintained at the pycnocline by deep turbulent mixing. The need for a much more detailed understanding of the linkage between subsurface Chl-a, pycnocline characteristics and deep turbulent processes is therefore a key subject, especially in highly productive but spatially heterogeneous areas such as shelf waters and shallow seas.

730 In the FoF and Tay region, Max  $N^2$  exhibited higher percentages of coincidence with CMDs (13.51% of 1273 profiles) than other DLs (Table 3). The depth of Max  $N^2$  is a less turbulent region where the energy to exchange parcels in the vertical is maximum (Boehrer and Schultze, 2009), and it is frequently used to identify the upper mixed layer. Oceanic sites exhibit phytoplankton blooms within the upper mixed layer (e.g. Behrenfeld, 2010; Costa et al., 2020; Somavilla et al., 2017) to coincide with AMLDs' vertical fluctuations due to e.g. windstorm events deepening the pycnocline into nutrient-enriched waters (Detoni et al., 2015; Carranza et al., 2018; Höfer et al., 2019; Montes-Hugo et al., 2009). In this study, all the investigated surface mixed layers' indicators (AMLD<sub>0.01</sub>, AMLD<sub>0.02</sub> and AMLD) weakly predicted DMC, reporting low linear correlations for all Chl-a shapes (Tables A1-A3 in Appendix A). The algorithm used in this study has reported an overall high performance in predicting the location of DMCs in HCU shape, which exhibited the shallowest DMCs (on average  $9.74 \pm 6.66$  m standard deviation). HCU shapes represent ephemeral surface blooms in shelf waters, whose DMCs resulted mainly at layers  $\leq$  the upper mixed layer depths. According to literature (Carranza et al., 2018; Zhao et al., 2019a), HCU showed the highest correlation to the upper mixed layer depth by exhibiting the largest percentage of DMCs above: AMLD<sub>0.1</sub> and AMLD<sub>0.2</sub> in 4.17% of the profiles, and AMLD in 25%. The AMLD identified by the proposed algorithm tested as the best variable in predicting most of DMCs in the one-to-one ( $R_0^2 = 0.76$ ) and empirical ( $R_{em}^2 = 0.34$ ) linear regressions, while BMLD accurately always defined the deepest boundary of DMCs in the observations (Table 4).

750 Since AMLD has been largely considered as a central variable for understanding phytoplankton dynamics (Sverdrup, 1953), it has been investigated in relation to climate change to infer possible significant changes in the amount, spatial distribution and phenology of oceanic primary production (Boyd et al., 2015; Montes-Hugo et al., 2009; Somavilla et al., 2017; Prend et al., 2019; Richardson and Bendtsen, 2019; Schmidt et al., 2020). However, the effect of climate change on AMLD and primary production is still an unsolved question (Lozier et al., 2011; Somavilla et al., 2017). The unclear effects of climate change on AMLD and primary production might be related to i) the difficulties in measuring the amount of subsurface Chl-a and its little association to satellites' observations at the sea surface (Baldry et al., 2020; Erickson et al., 2016; Lee et al., 2015), and ii) the exclusive investigation of the effects of surface mixing processes on primary production (e.g. temperature, wind-induced mixing) by neglecting deep processes that are responsible for the pycnocline's stability (Dave and Lozier, 2015, 2013; Lozier et al., 2011; Somavilla et al., 2017). As described above, the AMLD is informative for surface concentrations (HCU shapes), depth (e.g. Carvalho et al., 2017). The location of CMDs at Max  $N^2$

760 might reflect the distribution of phytoplankton within a less turbulent region where nutrient particles, which have been  
resuspended by mixing, can persist for longer time periods. The mild turbulent layer at Max  $N^2$  would therefore represent  
765 a hot spot of nutrients reached by resuspended phytoplankton cells, while strong mixing processes still undergoing above  
and/or below it, or diluted gradients of phytoplankton and nutrients throughout the water column, would avoid the creation  
of highly productive subsurface patches. However, the amount of standardized depth-integrated Chl-a below Max  $N^2$  is  
almost three times higher than above it (Table 4 and Fig. 5) suggesting that Max  $N^2$  is a layer of suitable conditions for  
770 phytoplankton to grow, but it lacks informing where most of the Chl-a vertically distribute. Although the depth of Max  
 $N^2$  appeared to inform better the exact location of CMDs, BMLD exhibited a clear pattern by distributing below CMD in  
78.32% of the profiles and representing the deepest limit up to which CMDs distributed. Overall, the linear correlation  
( $\rho_s$ ), the MA coefficients and the one-to-one linear regression  $R_0^2$  described a low association of CMDs with Max  $N^2$   
compared to HPDs' indicators and BMLD, and hence the use of Max  $N^2$  to locate subsurface Chl-a patches in summertime  
shelf waters may lead to underestimate the amount of Chl-a in the whole water column.

#### 4.2 Vertical distribution of Chl-a and BMLD

The observations carried out in the FoF and Tay region confirmed the subsurface presence of maxima Chl-a between  
775 April and August. A recent study in the German Bight described CMDs but it may not be biologically relevant for  
subsurface Chl-a that are maintained at the pycnocline by deep turbulent mixing. The need for a much more detailed  
understanding of the linkage between subsurface Chl-a, pycnocline characteristics and deep turbulent processes is  
therefore a key subject, especially in highly productive but spatially heterogeneous areas such as shelf waters and shallow  
seas.

#### 4.2 Association of subsurface Chl-a with DLs

780 The observations in the FoF and Tay region with a wide variety of characteristics of shallow seas, confirmed the  
subsurface presence of maxima Chl-a between April and August, with DMCs distributing on average ( $\pm$  standard  
deviation) at depths (m) equal to 17.22  $\pm$  4.95 in Wide-SCM, 15.08  $\pm$  4.47 in SCM-HCL, 14.82  $\pm$  3.29 in Narrow-SCM,  
22.69  $\pm$  10.91 in HCL, and 15.17  $\pm$  4.16 in SCM-HCU. A recent study in the German Bight described DMCs located  
785 mainly at the centre of the pycnocline and the overall amount of Chl-a at depths distinctly lower than the surface mixed  
layers (Zhao et al., 2019a). The vertical distribution of DMCs at BMLDs appeared to be correlated to the bathymetry by  
exhibiting DMCs closer to BMLDs at bathymetry comprised from, approximately, 40 to 70 m (in Narrow-SCM, SCM-  
HCL and Wide-SCM shapes), DMCs deeper than BMLD mainly in shallow waters (in HCL shapes, generally < 60 m),  
and DMCs above deep BMLD towards deeper waters (in SCM-HCU and HCU shapes, generally from 30 to 100 m) (Fig.  
790 A5-A in Appendix A). Previous studies identified a similar pattern in shallow waters where DMCs were mainly recorded  
at or below the base of the pycnocline (here BMLD) (Barth et al., 1998; Durán-Campos et al., 2019; Holligan et al., 1984;  
Zhao et al., 2019a). The link between bathymetry and Chl-a shapes, and the association of DMC with BMLD become  
important in those regions where bathymetry plays an important role in defining the location of commercial interests such  
as in the FoF and Tay region, location of several offshore wind farms ([www.marine.gov.scot](http://www.marine.gov.scot)). The installation feasibility  
will allow the deployment of wind turbines in water depths ranging from 41 to 58 m above the lowest astronomical tide  
795 (LAT) ([www.marine.gov.scot](http://www.marine.gov.scot)), where reliable environmental impact assessment, able to estimate the indirect effects in a  
holistic way, are required.

#### 4.2.1 Stable Chl-a shapes

Narrow and Wide SCM shapes can be considered as relatively stable vertical distribution of Chl-a since they occur during stable stratified conditions (Cullen, 2015; Carranza et al., 2018). DMCs at the pycnocline (between AMLD and BMLD) have been consistently recorded in Narrow SCM profiles within a pycnocline's width about  $8.81 \pm 3.83$  m on average ( $\pm$  standard deviation) (Fig. A4c in Appendix A). The location of DMC at the pycnocline in Narrow SCM The location of DMC at the pycnocline is regulated over time by upward nutrient-enriched fluxes entering the pycnocline from deep waters (Pingree et al., 1982; Rosenberg et al., 1990). In the Skagerrak strait between Denmark and Norway, deep SCMLs were recorded at a nutricline (rate of change in nitrate and phosphate) located below the base of a shallow pycnocline ( $< 15$  m) (Bjørnsen et al., 1993). A low number of Narrow SCM profiles exhibited DMCs deeper than BMLDs (8.42%), while this condition (DMC  $>$  BMLD) was more evident in Wide SCM profiles (16%) having a thicker and variable pycnocline (on average  $12.76 \pm 6.85$  m) than Narrow SCM profiles. The higher variability in the location of DMCs and BMLDs in Wide SCM ( $R_d^2 = 0.79$ ) than Narrow SCM ( $R_d^2 = 0.95$ ), and the extended distribution of Chl-a throughout the whole water column in Wide SCM might reflect a limited erosion of Chl-a by mixing and grazing above and below the pycnocline. Overall, the deep distribution of DMCs, and most of the depth-integrated Chl-a, in the proximity of the centre and the base of the pycnocline suggests the maintenance of subsurface Chl-a within shelf waters through the regulation of nutrient supply by deep physical processes.

#### 4.2.2 — Transient Chl-a shapes

Besides the stable Narrow and Wide SCM shapes, the other profiles (HCL, HCU, SCM-HCU and HCL) have been described in the literature as transient frames either from a stratified to a mixed water column or vice versa. Carranza et al. (2018) described two vertical distributions of Chl-a (from HCU to SCM-HCU) occurring from a mixed to stratified phase of the water column, indicating the ephemeral persistence of these shapes in the marine environment, eventually developing the typical (Narrow or Wide) SCM shapes. Although SCM-HCU and HCU profiles develop DMCs above AMLDs in Carranza et al. (2018), the observations in the FoF and Tay region reported DMCs deeper than AMLDs' indicators in  $> 62.50\%$  of HCU profiles and  $> 91.43\%$  of SCM-HCU (Fig. 6). Similarly to SCM-HCU, SCM-HCL might reflect the transition from stratified to mixed conditions, where phytoplankton cells concentrated at SCMLs are re-suspended and diluted in deep layers due to an increasing tidal current (Zhao et al., 2019a). Beside SCM-HCU and HCL might reflect different transitions between mixing and stratified conditions, only BMLD appeared a consistent proxy in defining the limit above which the DMCs have developed and, hence, is further discussed.

#### *SCM-HCU shape*

In SCM-HCU profiles, the DMCs occurred at  $\text{Max N}^2$  at a larger percentage (15.10% of the profiles) than the other density indicators. The low concentration of CMds below BMLD might reflect a limited erosion of Chl-a by mixing. The depth of  $\text{Max N}^2$  is a less turbulent region where the energy to exchange parcels in the vertical is maximum (Boehrer and Schultze, 2009), and it is frequently used to identify the upper mixed layer (e.g. Carvalho et al., 2017). The location of DMCs at  $\text{Max N}^2$  in SCM-HCU profiles might reflect the distribution of phytoplankton within a less turbulent region where nutrient particles, which have been resuspended by mixing, can persist for longer time periods. The mild turbulent layer at  $\text{Max N}^2$  would therefore represent a hot-spot of nutrients reached by resuspended phytoplankton cells, while strong mixing processes still undergoing above and/or below it, or diluted gradients of phytoplankton and nutrients throughout the water column, would avoid the creation of highly productive subsurface patches. Although the depth of  $\text{Max N}^2$  resulted in SCM-HCU being more informative than BMLD, DMCs exhibited a clear pattern by distributing shallower than BMLDs in 91.02% of the profiles and representing the deepest limit up to which DMCs distributed. Overall,  $\text{Max N}^2$  exhibited higher percentages of coincidence with DMCs (13.51% of 1273 profiles) than other DLs (Table 3), although the linear

840 correlation ( $\rho_S$ ), the MA coefficients and the one-to-one linear regression  $R_0^2$  described a low association of DMCs with Max  $N^2$  compared to HPDs' indicators and BMLD (Table 5 and Tables A4-A7 in Appendix A). However, the use of Max  $N^2$  in summertime shelf waters to infer the depth of subsurface Chl-a patches in a one-to-one fitting line (DMC = Max  $N^2$ ) may lead to underestimate the amount of Chl-a in the whole water column, as the amount of standardized depth-integrated Chl-a below Max  $N^2$  is almost three times higher than above it (Table 4 and Fig. A2 in Appendix A).

#### SCM-HCL shape

845 SCM-HCL exhibited a greater association of DMCs with BMLDs than HPDs' indicators or Max  $N^2$ , with the largest coincidence of DMC at BMLD (10.86% of the profiles) and  $\alpha$  and  $\beta$  coefficients from the Major Axis analysis close to a one-to-one fitting line (Table 5, Fig. 7). It was not the aim of this study to assess if the transient phase is taking place either from mixed to stratified waters or vice versa, although the closer proximity of DMCs to BMLDs than Max  $N^2$ , and the higher percentage of DMCs below Max  $N^2$  (73.09% of the profiles against 13.33% DMCs below BMLD) might indicate the erosion of a stable pycnocline where DMCs previously developed (transition from a stratified to a partially mixed water column). In the German Bight, 76% of SCM-HCL profiles presented high Chl-a at the base of the SCMLs, suggesting a possible erosion of the subsurface layer from the bottom due to strong tidal currents (Zhao et al., 2019a). The physical factors developing SCM-HCL might not cause the mixing of the whole water column and, instead, sustain an indispensable upward flux of nutrients into the enduring pycnocline, where e.g. and grazing (Benoit-Bird et al., 2013). The physical factors developing subsurface Chl-a are defined by mixing processes below the pycnocline that provides an indispensable upward flux of nutrients in the euphotic zone, where e.g. dinoflagellates are able to compete successfully in slightly turbulent conditions ( $< 0.1 \text{ mm s}^{-1}$ ) (Ross and Sharples, 2007). Therefore, the erosion as well as the resuspension of previously sinking phytoplankton cells and nutrients can maintain the proximity of DMCs at BMLDs. Although SCM-HCL appears to be a transient shape with a short life (Zhao et al., 2019a), it has been widely encountered ( $n=405$ ) during summer in the FoF and Tay region, and therefore its permanency might occur at a temporal scale (e.g. spring-neap cycle) that allows phytoplankton to counteract the dispersion of the gradients. Moreover, the large amount of diluted Chl-a in deep waters (64.17% of depth-integrated Chl-a below BMLD, Fig. 6) therefore, the erosion as well as the resuspension of sinking phytoplankton cells and nutrients can maintain the proximity of CMs at BMLDs setting the location of the nutricline at the base of the pycnocline. It is also noticeable that a large amount of diluted Chl-a in deep waters (51.67% of depth-integrated Chl-a below BMLD) might be crucial in maintaining primary production at the subsurface over the summer, since deep mixing processes eroding and sustaining Chl-a at BMLD would contribute also to reducing the overlap between SCMLs and predators (Behrenfeld, 2010) (Behrenfeld, 2010).

865 Overall, the deep distribution of CMs, and most of the depth-integrated Chl-a, in the proximity of the centre and the base of the pycnocline suggests the maintenance of subsurface Chl-a within shelf waters through the regulation of nutrient supply by waters below the pycnocline and makes this linkage responsive to variations in deep physical processes.

#### 4.3 Using BMLD to investigate impacts on primary production

870 The marine photosynthetic activity represents an essential biological pump of carbon sequestration (Boyd et al., 2015), whose extent is often invalidated by the exclusion of subsurface Chl-a of up to 10%-40% (Sharples et al., 2001). The correct measurement of primary production throughout the whole water column is essential to address which factors affect absorbing atmospheric carbon dioxide in the marine environment. Recent studies reported a decrease of Chl-a biomass (Capuzzo et al., 2018; Schmidt et al., 2020) and a temporal shift of phytoplankton bloom (Silva et al., 2021) due to significant changes in the surface MLD. The Northeast Atlantic shelves experienced a summertime reduction of Chl-a in

ha formattato: Colore carattere: Evidenziatore 1

880 the last 60 years leading to significant impacts on the food web, caused by an intensified stratification of the water column that maintains nutrient fluxes in deep waters (Capuzzo et al., 2018; Schmidt et al., 2020). Prolonged stratified conditions were reported to define deeper concentrated patches of Chl-a (Somavilla et al., 2017; Scott et al., 2010), where phytoplankton stabilize at deep low-turbulence layers (Bopp et al., 2013) having still sufficient light to photosynthesize and set the nitracline position. The starvation of nutrients at surface force phytoplankton to re-distribute in the water column (e.g. Bindoff et al., 2019; Boyd et al., 2015; Schmidt et al., 2020) in deeper nutrient-enriched waters within the euphotic zone. Hence, the location of CMds in the proximity of the deepest portion of the pycnocline, between  $HPD_{AML,D}$ ,  $BMLD$  and  $BMLD$ , (78.32% of the profiles) is not surprising during summer in the Firth of Forth and Tay regions. Although a consistent portion of depth-integrated Chl-a is reported below pycnocline, the vertical distribution of  $BMLD$  resulted in setting the position of subsurface productive patches in stratified waters, representing an important indicator of the vertical distribution of phytoplankton in shelf waters.

885 The effects of an intensified stratification on primary production in the continental shelf waters are still entangled and suggest an overall deepening of subsurface Chl-a, which is likely to delineate a knock-on effect on redistributing most of the higher trophic levels (e.g., zooplankton, fish) and affect the foraging success of highly adapted species. However, the deepening of productive patches is difficult to examine over large spatial scales, and remote sensing methods often lack reliability for subsurface data. The role of climate change in increasing stratification are likely to affect the distribution of  $BMLD$  and the upward fluxes, which may either redistribute food patches at major depths together with the deepening of  $BMLD$  and causing an overall reduction of primary production or shifts of community compositions.

895 **4.2.3**—It is hence reasonable to notice that the potential effects on primary production involves both surface and deep (below the pycnocline) processes, especially where multiple local changes (i.e. wind turbine foundations changing levels of mixing) repeated over large spatial areas (i.e. the North Sea) have an effect at different scales (van der Molen et al., 2014; De Dominicis et al., 2018; Carpenter et al., 2016). The upcoming interest of the offshore renewable sector in building offshore wind farms (OWFs) in the FoF and Tay region (www.marine.gov.scot) rises the need of drafting reliable environmental impact assessments able to identify key variables for estimating the effects in a holistic way. The consequences of offshore wind farms are likely to be related to bathymetry and mixing budgets, by affecting the stratification rate differently across several bathymetries. The vertical distribution of CMds at  $BMLDs$  appeared to be correlated to the bathymetry by exhibiting CMds closer to  $BMLDs$  at water depths comprised from, approximately, 40 to 70 m. CMds deeper than  $BMLD$  mainly in shallow waters < 60 m, and CMds above  $BMLD$  towards deeper waters up to 100 m (Fig. A3 in Appendix A). **HCL shape and  $BMLD$  in shallow waters**

900 The opposite condition is found in HCL profiles, where DMcs have been identified in deep layers below  $BMLD$  in 87.14% profiles (Table 4). The large portion of deep Chl-a, which is typical in HCL shapes, is described in the literature as primary production trapped in deep waters by a surface layer with a low diffusivity (e.g. pycnocline) (Jones et al., 1998; Zhao et al., 2019a). Besides the potential physical drivers inducing Chl-a below  $BMLD$  (77.24% of depth integrated Chl-a is below  $BMLD$ , Fig. 6), deep Chl-a is probably accumulated due to the slowdown of the current at the seabed (Neill and Hashemi, 2018). In particular significantly more HCL profiles (results in Sect. 3.3.1) have been recorded in shallow waters (from 22.45 to 63.15 m, on average  $30.77 \pm 11.59$  m, Fig. A5b in Appendix A) as well as in other studies (Jones et al., 1998; Huisman et al., 2002; Zhao et al., 2019a), where a compatible amount of light and suspended sediments can sustain phytoplankton growth throughout most of the water column (Huisman et al., 2002). Although sinking rates have been described as the main driver of Chl-a distribution below  $BMLD$  (Jones et al., 1998; Huisman et al., 2002; Zhao

et al., 2019a), the density at DMCs showed a similar range (1021–1028 kg m<sup>-3</sup>) to the other Chl a shapes exhibiting deep DMCs below BMLD (Wide SCM, SCM HCL) (Fig. A4a and Table A8 in Appendix A report no significant differences between these shapes), suggesting that hydrodynamic drivers (e.g. deep turbulent nutrient enriched fluxes) might have more of an effect on Chl a profiles than density on sinking rates. Another characteristic of the HCL shape is the exceptionally high concentration of Chl a at DMCs than all the other profiles (results in Sect. 3.3.1, and Fig. A4b in Appendix A). It is evident that HCL profiles occurred at stratified conditions, probably when the tidal speed was slow enough to allow the stratification to persist (Zhao et al., 2019a) below a thin pycnocline (on average  $8.82 \pm 5.19$  m, Fig. A4c in Appendix A) able to trap down a significantly large amount of Chl a over shallow regions. Therefore, the provenance of high Chl a at depth in shallow regions ( $\leq 63$  m) might be due to the passive drift and accumulation by horizontal tidal currents in shallow waters, or the sinking combined with resuspension and active photosynthesis. Overall, high concentrations of Chl a below the pycnocline represented a distinct pattern in shallow waters, revealing the sensitivity of these regions to further changes in the stratification strength or mixing at a small scale ( $< 1$  km) of the water column due to manmade structures (e.g. renewable deployments).

#### 4.3 The role of BMLD in further climate change investigations

Regions with large and deep phytoplankton concentrations are highly important for absorbing and sinking atmospheric carbon dioxide and represent a biological pump of carbon sequestration (Boyd et al., 2015). The correct estimation of the abundance of subsurface primary production is therefore highly important in investigating climate change implications in the marine environment. The exclusion of subsurface Chl a in shelf waters is estimated to undervalue the total productivity of up to 10%–40% (Sharples et al., 2001). This amount of underestimation and lack of understanding of exact mechanisms for changes in vertical location of density and Chl a would strongly affect the wider scale assessment of climate change impacts as well as the finer scale of manmade structures on the biological functionality of a certain region. The location of the BMLD was overall the best variable constantly informing about the locations of DMCs throughout the water column. However, we want to highlight that a minimum of 39% of depth integrated Chl a is found within waters below the BMLD and this represents a high proportion of potential primary production that needs to be considered. In terms of abundance of primary production, the Northeast Atlantic shelves exhibited a summertime reduction of Chl a in the last 60 years leading to significant impacts on the food web in the North Sea (Capuzzo et al., 2018; Schmidt et al., 2020). In particular, the intensified stratification caused an effective reduction in nutrient supply at the surface with the consequential starvation and change of phytoplankton communities (e.g. Bindoff et al., 2019; Boyd et al., 2015; Schmidt et al., 2020). The isolation of surface waters from deep nutrient rich waters may explain the distribution of phytoplankton at the subsurface, especially in the proximity of BMLD, which represents the limits up to which the deep nutrient enriched fluxes distribute and allows phytoplankton to grow in a region with low turbulence (Bopp et al., 2013; Boyd et al., 2015). Not only the stratification strengthening but also the vertical distribution of BMLD and the upward fluxes, up to the pycnocline may either redistribute food patches at major depths, together with the deepening of BMLD, and causing an overall reduction of primary production or community's shift due to the reduced light at depth.

Investigating the potential effects of climate change involves not only surface processes, but also deep systems at the large and local scales, especially where multiple local changes (i.e. wind turbine deployments changing levels of mixing) repeated over large spatial areas (i.e. the North Sea) are likely to have an effect at different scales (van der Molen et al., 2014; De Dominicis et al., 2018). Long term effects of variations in deep mixing processes appear essential to assess shelf seas at a regional scale, leading to identifying key indicators, or sensitive links, of subsurface highly productive

955 patches at a fine scale. The physical processes delineating the vertical distribution of density therefore represented a valuable tool in identifying possible biases or underestimations of Chl-a contents in shelf waters.

960 Previous studies identified a similar pattern in shallow waters where CMDs were mainly recorded at or below the base of the pycnocline (Barth et al., 1998; Durán-Campos et al., 2019; Holligan et al., 1984; Zhao et al., 2019a). Although stratification is reported to intensify in shelf waters with climate change, the increase in turbulence downstream wind farms may counteract the local stratification (Carpenter et al., 2016; Schullien et al., 2017; Schultze et al., 2020) and affect the temporal and spatial distribution of Chl-a. Since the variation in stratification is a useful tool to address possible impacts on primary production, using BMLD is likely to be more efficient in predicting changes in the vertical distribution of Chl-a and its possible consequences. The deepening of BMLD within or even below the euphotic zone may lead Chl-a to decrease across shelf seas since phytoplanktonic cells would buoyance at deeper and darker depths. Hence, the use of AMLD to investigate physical alteration of climate change and man-made structures should be integrated with the use of BMLD and the understanding of physical processes at depth, together with changes in seabed temperature, and the slow down or increase of upward fluxes.

## 5. Conclusion

970 Chl-a vertical distribution (here classified as shapes) gives important information about the state of development of the phytoplankton community and their reliance on nutrient gradients that are likely to be, which is associated with mixed and stratified layers. The upper and deep mixing processes above and below the pycnocline can have very different influences on the Chl-a vertical distribution, dictating the concentration at subsurface patches that can distribute close to, above, or below the pycnocline.

975 The Although the association of phytoplankton with AMLD has been largely described at large spatial scales within oceanic habitats. This, the presented study shows there is a very weak linkage between AMLD and CMD in shelf waters, at a very high vertical resolution (vertical samples at 1 m distances), compared to HPDs' indicators or BMLD, which has led us to hypothesize that, at fine spatial scales, in shallow shelf seas, there is a stricter association of summertime subsurface patches of Chl-a with the bottom half of the pycnocline. Therefore bottom deep mixing processes (e.g., such as tidal eyes) may currents in the North Sea, play a role in regulating summertime subsurface primary production in shelf waters and may regulate their distribution at BMLDs in stratified conditions. Considering the described associations of subsurface Chl-a with BMLD provided by this study, it is evident how this new level of understanding variable can play a role in the assessment of productivity, since the bottom deep mixing processes may be more (or are equally (or more) relevant than the surface process in determining a shift of primary production at a local (due to e.g. the increase of mixing downstream a wind turbine deployment) local or large scales (e.g. due to climate change). This association therefore advocates the investigation of the effect of anomaly-inducing processes occurring at and below the pycnocline (e.g. bottom deep sea temperature, bottom deep salinity, turbulence and physical processes at the BMLD), which are likely to influence primary production and the whole ecosystem dynamics within shelf seas (Trifonova et al., 2021). The new understanding of Understanding mechanisms affecting primary production at fine scales may be very important to investigate as we are moving rapidly towards the deployment of thousands of wind turbine foundations and 100s of hundreds GW of in the wind energy extraction sector from worldwide shallow seas (Gielen et al., 2019)(Gielen et al., 2019). Hence, BMLD is proposed as an ecological relevant variable for further oceanographic investigations in shelf waters, and the proposed approach is a valuable tool to extrapolate this variable from *in situ* vertical samples.

Appendix A

995

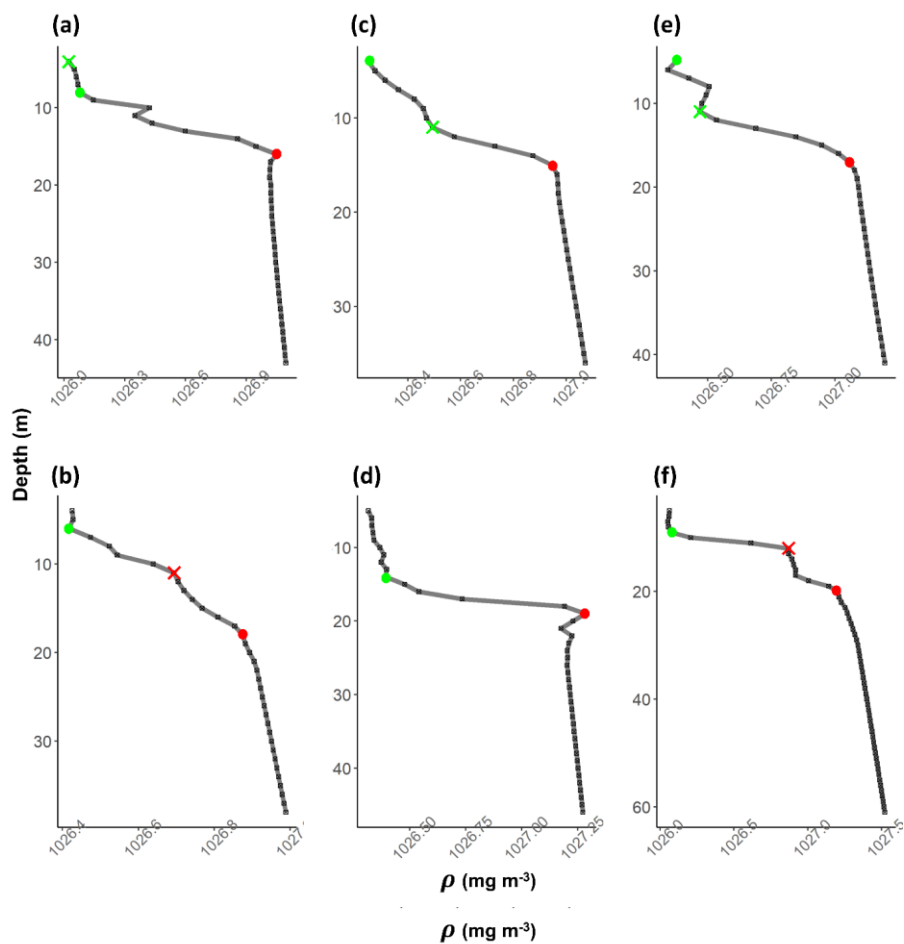
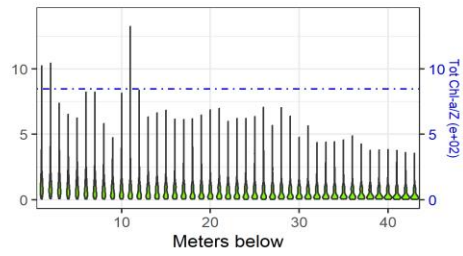
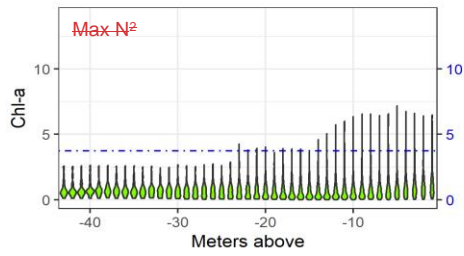
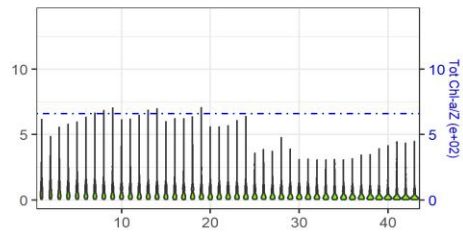
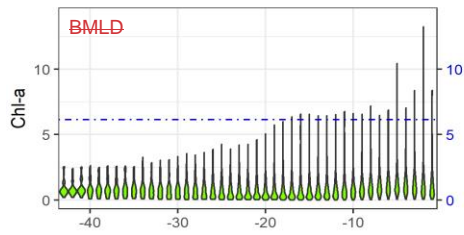
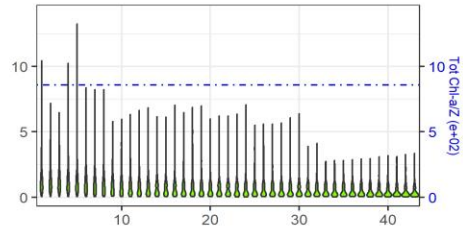
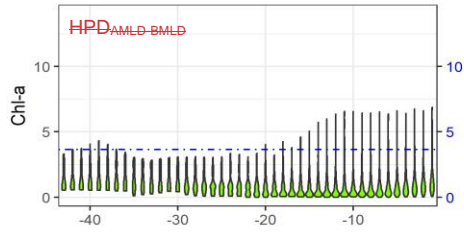
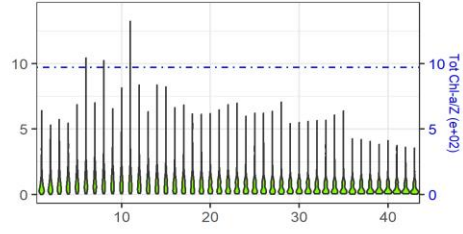
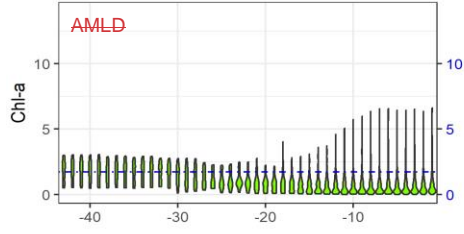


Figure A1: ~~Exampleexamples~~ of density profiles (grey line) (a-f). The black squares are the values at 1 m resolution. Red dots refer to BMLD, green dots to AMLD. Crosses refer to misidentified AMLD (in green) and BMLD (in red) that needed to be manually corrected.

1000

ha formattato: Tipo di carattere: Non Corsivo  
 Formattato: Didascalia, Allineato al centro



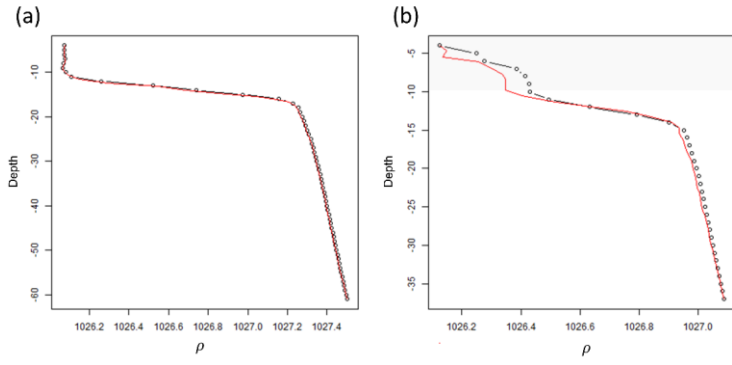


Figure A2: Violin plot of the amount of Chl-a (mg) at each meter above and below the four two density layers (AML<sub>D</sub>, HPD<sub>AML<sub>D</sub>-BML<sub>D</sub></sub>, BML<sub>D</sub> and Max N<sup>2</sup>) from the whole dataset. The dot-dashed blue lines represent the depth-integrated Chl-a measured as the total amount of Chl-a (mg) divided by the number of depths ( $\bar{z}$ ) within each portion of the water column (meters above and meters below DLs) (values are reported in Table 2).

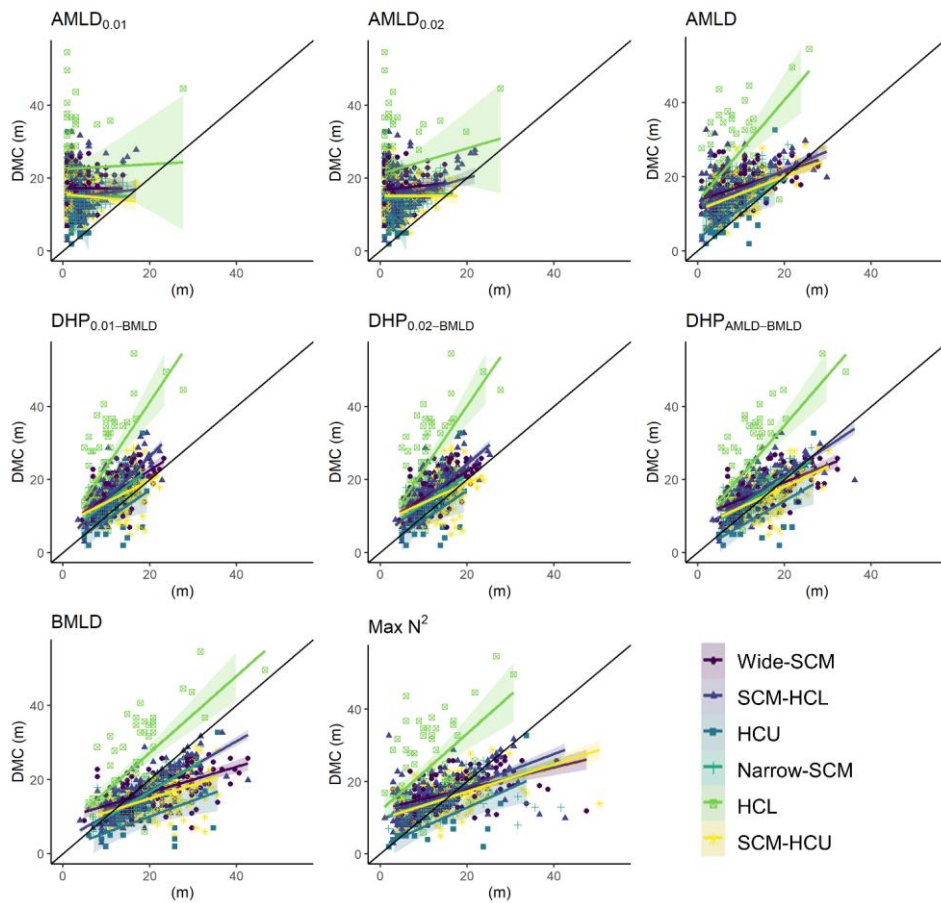


Figure A3: Plots of DMCs against the eight investigated density layers, profiles whose observations are coloured by Chl-a vertical shape. Coloured lines refer to the empirical linear regression ( $DMC \sim DL$ ), while the were standardized at equals 1 m depths using generalized additive model (GAM). (a) reports a density profile (black dotted line) where GAM correctly fitted (red solid line-is) the one-to-one fitting line ( $DMC = DL$ ).

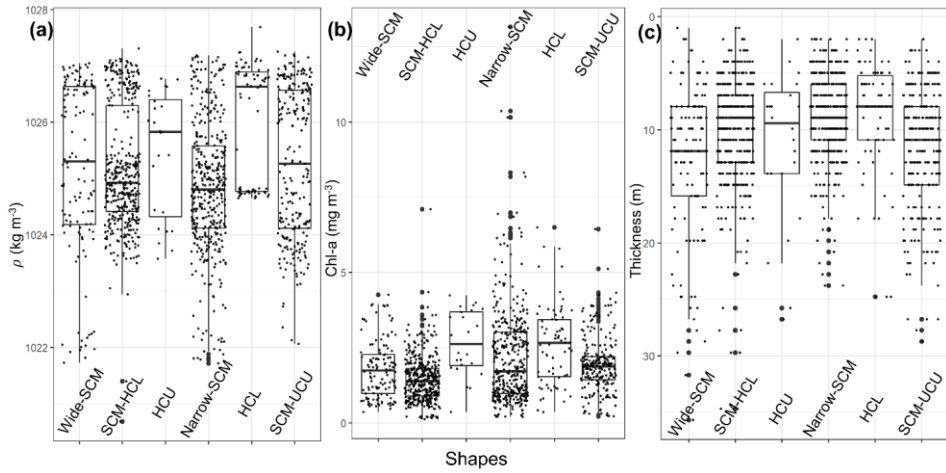


Figure A4: Boxplots of (vertical distribution, (b) reports a) density at DMCs, (b) Chl-a at DMCs, and (c) the thickness of pycnoclines (measured as the difference between AMLD and BMLD) for each Chl-a shape-profile where GAM wrongly fitted the upper portion of the profile (grey polygon area) and, hence, required a manual correction of the values.

1025

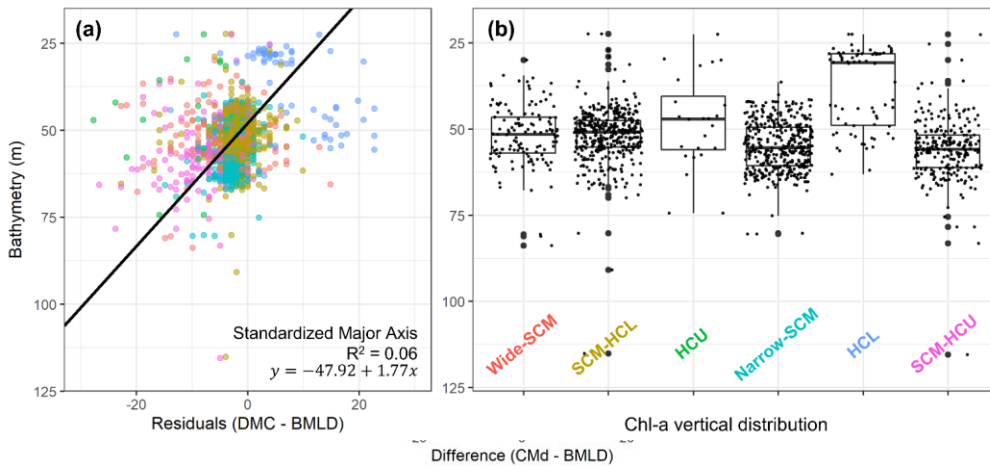


Figure A5: (a) scatterplot of the residuals measured as the difference between DMC and BMLD (one-to-one fitting line,  $DMC=BMLD$ ), against the bathymetry at which each profile was sampled. (b) The solid black line reports a Standardized Major Axis analysis. Colours refer to Chl-a shape, whose ranges of bathymetry equation and  $R^2$  squared values are reported.

1030

Tables A1-A7: Statistical parameters and percentages of the observations categorized by ChI-a vertical shape exhibiting DMCs above ( $>$ ), at the same depth ( $=$ ), or below ( $<$ ) the  $AML D_{0.01}$  (Table A1),  $AML D_{0.02}$  (Table A2),  $AML D$  (Table A3),  $HPD_{0.01-BMLD}$  (Table A4),  $HPD_{0.02-BMLD}$  (Table A5),  $HPD_{AML D-BMLD}$  (Table A6), and  $Max-N^2$  (Table A7).

Table A1

DL = $AML D_{0.01}$								
ChI-a shape	$\rho_{\mathcal{Y}}$	$\alpha$	$\beta$	$R_{\mathcal{G}}^2$	$R_{\mathcal{G}M}^2$	DMC > DL	DMC = DL	DMC < DL
Wide-SCM	0.00	21339.29	-5546.12	0.35	0.00	100	0.00	0.00
SCM-HCL	0.07	-83.35	24.55	0.41	0.00	100	0.00	0.00
HCU	-0.18	68.85	-23.09	0.27	0.03	79.17	16.67	4.17
Narrow-SCM	0.02	-127.00	28.14	0.51	0.00	100	0.00	0.00
HCL	0.02	-436.78	129.32	0.22	0.00	100	0.00	0.00
SCM-HCU	-0.07	68.89	-13.77	0.38	0.01	99.59	0.41	0.00

Table A2

DL = $AML D_{0.02}$								
ChI-a shape	$\rho_{\mathcal{Y}}$	$\alpha$	$\beta$	$R_{\mathcal{G}}^2$	$R_{\mathcal{G}M}^2$	DMC > DL	DMC = DL	DMC < DL
Wide-SCM	0.08	-32.36	11.67	0.38	0.01	100	0.00	0.00
SCM-HCL	0.24	-0.27	3.12	0.49	0.06	100	0.00	0.00
HCU	-0.18	69.85	-22.75	0.28	0.03	79.17	16.67	4.17
Narrow-SCM	0.09	6.51	1.30	0.61	0.01	100	0.00	0.00
HCL	0.13	-49.80	16.96	0.27	0.02	100	0.00	0.00
SCM-HCU	0.00	776.92	-158.95	0.45	0.00	99.18	0.00	0.82

Table A3

DL = $AML D$								
ChI-a shape	$\rho_{\mathcal{Y}}$	$\alpha$	$\beta$	$R_{\mathcal{G}}^2$	$R_{\mathcal{G}M}^2$	DMC > DL	DMC = DL	DMC < DL
Wide-SCM	0.48	10.88	0.69	0.70	0.23	91.20	1.60	7.20
SCM-HCL	0.51	7.76	1.04	0.66	0.26	98.52	0.49	0.99
HCU	0.58	-3.77	1.73	0.76	0.34	62.50	12.50	25.00
Narrow-SCM	0.41	7.40	0.88	0.77	0.17	98.76	1.24	0.00
HCL	0.55	-4.23	3.97	0.47	0.31	98.57	0.00	1.43
SCM-HCU	0.51	8.00	0.79	0.77	0.26	91.43	4.08	4.49

Table A4

DL = $HPD_{AML D-0.01-BMLD}$								
ChI-a shape	$\rho_{\mathcal{Y}}$	$\alpha$	$\beta$	$R_{\mathcal{G}}^2$	$R_{\mathcal{G}M}^2$	DMC > DL	DMC = DL	DMC < DL
Wide-SCM	0.60	-1.68	1.46	0.89	0.36	88.80	1.60	9.60
SCM-HCL	0.75	-4.06	1.81	0.88	0.57	95.31	1.98	2.72

HCU	0.52	-14.66	2.24	0.76	0.27	41.67	4.17	54.17
Narrow-SCM	0.64	-5.18	1.79	0.91	0.41	94.31	1.49	4.21
HCL	0.65	-14.46	3.88	0.61	0.43	97.14	0.00	2.86
SCM-HCU	0.43	-9.78	2.03	0.90	0.19	78.37	2.45	19.18

Table A5

DL = HPD <sub>AMLD-0.02-BMLD</sub>								
Chl-a shape	$\rho_x$	$\alpha$	$\beta$	$R_U^2$	$R_{DM}^2$	DMC > DL	DMC = DL	DMC < DL
Wide-SCM	0.61	-0.61	1.36	0.90	0.37	87.20	2.40	10.40
SCM-HCL	0.74	-1.55	1.51	0.90	0.56	94.07	2.72	3.21
HCU	0.52	-14.68	2.23	0.76	0.27	41.67	4.17	54.17
Narrow-SCM	0.61	-3.03	1.51	0.93	0.37	86.88	5.45	7.67
HCL	0.67	-12.50	3.54	0.63	0.45	97.14	0.00	2.86
SCM-HCU	0.43	-7.01	1.74	0.91	0.18	73.88	4.49	21.63

1045

Table A6

DL = HPD <sub>AMLD-BMLD</sub>								
Chl-a shape	$\rho_x$	$\alpha$	$\beta$	$R_U^2$	$R_{DM}^2$	DMC > DL	DMC = DL	DMC < DL
Wide-SCM	0.60	6.65	0.68	0.91	0.36	66.40	1.60	32.00
SCM-HCL	0.74	2.20	1.07	0.92	0.56	87.65	3.95	8.40
HCU	0.62	-6.13	1.17	0.68	0.38	20.83	4.17	75.00
Narrow-SCM	0.71	0.22	1.13	0.96	0.50	75.25	5.94	18.81
HCL	0.69	-5.74	2.54	0.69	0.48	95.71	0.00	4.29
SCM-HCU	0.59	1.68	0.91	0.94	0.35	56.73	6.53	36.73

Table A7

DL = Max N <sup>2</sup>								
Chl-a shape	$\rho_x$	$\alpha$	$\beta$	$R_U^2$	$R_{DM}^2$	DMC > DL	DMC = DL	DMC < DL
Wide-SCM	0.51	10.95	0.37	0.83	0.26	56.00	5.60	38.40
SCM-HCL	0.63	7.57	0.61	0.88	0.39	73.09	13.83	13.09
HCU	0.55	4.42	0.34	-0.11	0.31	16.67	16.67	66.67
Narrow-SCM	0.55	7.82	0.52	0.92	0.30	64.85	16.58	18.56
HCL	0.56	-5.84	2.82	0.62	0.31	95.71	1.43	2.86
SCM-HCU	0.55	7.52	0.52	0.89	0.30	52.24	15.10	32.65

Table A8: Wilcoxon test between the density at DMCs in HCL shape and all the other Chl-a shapes. In bold the Chl-a shapes having density at DMCs significantly different from HCL profiles.

1050

Shape vs HCL	W	p
Wide-SCM	4375	0.289
SCM-HCL	15624	0.062

HCU	1075	0.126
Narrow-SCM	19592	0.023
SCM-HCU	11824	0.000

#### Author contribution

Arianna Zampollo contributed to the conceptualization of the study, formal analyses, methodology on AMLD and BMLD, writing of the original draft, and software use; Thomas Cornulier contributed to the conceptualization and supervision of the statistical method, writing of the original draft, methodology and visualization of the results; Rory O'Hara Murray contributed on the data curation, writing of the original draft, supervision, visualization and validation; Jacqueline F. Tweddle contributed to the conceptualization and the supervision of the study; James Dunning contributed to the methodology of the AMLD and BMLD algorithm; Beth Scott contributed to the conceptualization of the analyses, writing of the original draft, supervision, funding acquisition, resources and data curation.

#### Code availability

The code for the AMLD and BMLD algorithm are available [upon request to zampolloarianna@gmail.com](mailto:upon-request-to-zampolloarianna@gmail.com) <https://github.com/azampollo/BMLD>

#### Data availability

Data are available upon request and agreement with the co-authors.

#### Competing interests

The authors declare that they have no conflict of interest.

#### Acknowledgment

The authors thank the founding MarCRF, the Marine Collaboration Research Forum jointly sponsored by the University of Aberdeen and Marine Scotland Science, and Marine Scotland Science to provide a portion of the data.

#### References

Baetge, N., Graff, J. R., Behrenfeld, M. J., and Carlson, C. A.: Net Community Production, Dissolved Organic Carbon Accumulation, and Vertical Export in the Western North Atlantic, *Front. Mar. Sci.*, 7, 227, <https://doi.org/10.3389/fmars.2020.00227>, 2020.

Baldry, K., Stratton, P. G., Hill, N. A., and Boyd, P. W.: Subsurface Chlorophyll-a Maxima in the Southern Ocean, *Front. Mar. Sci.*, 7, 671, <https://doi.org/10.3389/fmars.2020.00671>, 2020.

Banse, K.: Clouds, deep chlorophyll maxima and the nutrient supply to the mixed layer of stratified water bodies, *J. Plankton Res.*, 9, 1031–1036, <https://doi.org/10.1093/plankt/9.5.1031>, 1987.

Barth, J. A., Bogucki, D., Pierce, S. D., and Kosro, P. M.: Secondary circulation associated with a shelfbreak front, *Geophys. Res. Lett.*, 25, 2761–2764, <https://doi.org/10.1029/98GL02104>, 1998.

Behrenfeld, M. J.: Abandoning Sverdrup's Critical Depth Hypothesis on phytoplankton blooms, *Ecology*, 91, 977–989, <https://doi.org/10.1890/09-1207.1>, 2010.

ha formattato: Tipo di carattere: +Corpo (Calibri), 11 pt

Benoit-Bird, K. J., Shroyer, E. L., and McManus, M. A.: A critical scale in plankton aggregations across coastal ecosystems: [CRITICAL SCALE IN PLANKTON AGGREGATIONS](https://doi.org/10.1002/grl.50747), *Geophys. Res. Lett.*, 40, 3968–3974, <https://doi.org/10.1002/grl.50747>, 2013.

ha formattato: Tipo di carattere: +Corpo (Calibri), 11 pt

1085 Bindoff, N. L., Cheung, W. W. L., Kairo, J. G., Aristegui, J., Guinder, V. A., Hallberg, R., Hilmi, N., Jiao, N., O'Donoghue, S., Suga, T., Acar, S., Alava, J. J., Allison, E., Arbic, B., Bambridge, T., Boyd, P. W., Bruggeman, J., Butenschön, M., Chávez, F. P., Cheng, L., Cinar, M., Costa, D., Defeo, O., Djoundourian, S., Domingues, C., Eddy, T., Endres, S., Fox, A., Free, C., Frölicher, T., Gattuso, J.-P., Gerber, G., Hallegraef, G., Harrison, M., Hennige, S., Hindell, M., Hogg, A., Ito, T., Kenny, T.-A., Kroeker, K., Kwiatkowski, L., Lam, V. W. Y., Laüfkotter, C., LeBillon, P., Bris, N. L., Lotze, H., MacKinnon, J., de Marffy-Mantuano, A., Martel, P., Molinos, J. G., Moseman-Valtierra, S., Motau, A., Mulsow, S., Mutombo, K., Oyinlola, M., Poloczanska, E. S., Pascal, N., Philip, M., Purkey, S., Rathore, S., Rebelo, X., Reygondeau, G., Rice, J., Richardson, A., Riebesell, U., Roach, C., Rocklöv, J., Roberts, M., Sloyan, B., Smith, M., Shurety, A., Wabnitz, C., and Whalen, C.: Changing Ocean, Marine Ecosystems, and Dependent Communities, *Mar. Ecosyst.*, 142, n.d.

1095 Bjørnson, P., Kaas, H., Kaas, H., Nielsen, T., Olesen, M., and Richardson, K.: Dynamics of a subsurface phytoplankton maximum in the Skagerrak, *Mar. Ecol. Prog. Ser.*, 95, 279–294, <https://doi.org/10.3354/meps095279>, 1993.

1100 Boehrer, B. and Schultze, M.: Density Stratification and Stability, in: *Encyclopedia of Inland Waters*, edited by: Likens, G. E., Academic Press, Oxford, 583–593, <https://doi.org/10.1016/B978-012370626-3.00077-6>, 2009.

[Bonaduce, A., Staneva, J., Behrens, A., Bidlot, J.-R., and Wilcke, R. A. I.: Wave Climate Change in the North Sea and Baltic Sea, \*J. Mar. Sci. Eng.\*, 7, 166, <https://doi.org/10.3390/jmse7060166>, 2019.](https://doi.org/10.3390/jmse7060166)

1105 Bopp, L., Resplandy, L., Orr, J. C., Doney, S. C., Dunne, J. P., Gehlen, M., Halloran, P., Heinze, C., Ilyina, T., Séférian, R., Tjiputra, J., and Vichi, M.: Multiple stressors of ocean ecosystems in the 21st century: projections with CMIP5 models, *Biogeosciences*, 10, 6225–6245, <https://doi.org/10.5194/bg-10-6225-2013>, 2013.

ha formattato: Tipo di carattere: +Corpo (Calibri), 11 pt

Boyd, P. W., Lennartz, S. T., Glover, D. M., and Doney, S. C.: Biological ramifications of climate-change-mediated oceanic multi-stressors, *Nat. Clim. Change*, 5, 71–79, <https://doi.org/10.1038/nclimate2441>, 2015.

1110 Brown, Z. W., Lowry, K. E., Palmer, M. A., van Dijken, G. L., Mills, M. M., Pickart, R. S., and Arrigo, K. R.: Characterizing the subsurface chlorophyll a maximum in the Chukchi Sea and Canada Basin, *Deep Sea Res. Part II Top. Stud. Oceanogr.*, 118, 88–104, <https://doi.org/10.1016/j.dsr2.2015.02.010>, 2015.

[Bryden, H. L., Longworth, H. R., and Cunningham, S. A.: Slowing of the Atlantic meridional overturning circulation at 25° N, \*Nature\*, 438, 655–657, <https://doi.org/10.1038/nature04385>, 2005.](https://doi.org/10.1038/nature04385)

1115 Capuzzo, E., Lynam, C. P., Barry, J., Stephens, D., Forster, R. M., Greenwood, N., McQuatters-Gollop, A., Silva, T., Leeuwen, S. M. van, and Engelhard, G. H.: A decline in primary production in the North Sea over 25 years, associated with reductions in zooplankton abundance and fish stock recruitment, *Glob. Change Biol.*, 24, e352–e364, <https://doi.org/10.1111/gcb.13916>, 2018.

ha formattato: Tipo di carattere: +Corpo (Calibri), 11 pt

1120 [Carpenter, J. R., Merckelbach, L., Callies, U., Clark, S., Gaslikova, L., and Baschek, B.: Potential Impacts of Offshore Wind Farms on North Sea Stratification, \*PLOS ONE\*, 11, e0160830, <https://doi.org/10.1371/journal.pone.0160830>, 2016.](https://doi.org/10.1371/journal.pone.0160830)

Carranza, M. M., Gille, S. T., Franks, P. J. S., Johnson, K. S., Pinkel, R., and Girton, J. B.: When Mixed Layers Are Not Mixed. Storm-Driven Mixing and Bio-optical Vertical Gradients in Mixed Layers of the Southern Ocean, *J. Geophys. Res. Oceans*, 123, 7264–7289, <https://doi.org/10.1029/2018JC014416>, 2018.

ha formattato: Tipo di carattere: +Corpo (Calibri), 11 pt

- 1125 Carvalho, F., Kohut, J., Oliver, M. J., and Schofield, O.: Defining the ecologically relevant mixed-layer depth for Antarctica's coastal seas, *Geophys. Res. Lett.*, 44, 338–345, <https://doi.org/10.1002/2016GL071205>, 2017.
- Chiswell, S. M.: Annual cycles and spring blooms in phytoplankton: don't abandon Sverdrup completely, *Mar. Ecol. Prog. Ser.*, 443, 39–50, <https://doi.org/10.3354/meps09453>, 2011.
- 1130 Chu, P. C. and Fan, C.: Maximum angle method for determining mixed layer depth from seaglider data, *J. Oceanogr.*, 67, 219–230, <https://doi.org/10.1007/s10872-011-0019-2>, 2011.
- Chu, P. C. and Fan, C.: Global ocean synoptic thermocline gradient, isothermal-layer depth, and other upper ocean parameters, *Sci. Data*, 6, 119, <https://doi.org/10.1038/s41597-019-0125-3>, 2019.
- 1135 Costa, R. R., Mendes, C. R. B., Tavano, V. M., Dotto, T. S., Kerr, R., Monteiro, T., Odebrecht, C., and Secchi, E. R.: Dynamics of an intense diatom bloom in the Northern Antarctic Peninsula, February 2016, *Limnol. Oceanogr.*, 65, 2056–2075, <https://doi.org/10.1002/lno.11437>, 2020.
- Courtois, P., Hu, X., Pennelly, C., Spence, P., and Myers, P. G.: Mixed layer depth calculation in deep convection regions in ocean numerical models, *Ocean Model.*, 120, 60–78, <https://doi.org/10.1016/j.ocemod.2017.10.007>, 2017.
- 1140 Cullen, J. J.: Subsurface Chlorophyll Maximum Layers: Enduring Enigma or Mystery Solved?, *Annu. Rev. Mar. Sci.*, 7, 207–239, <https://doi.org/10.1146/annurev-marine-010213-135111>, 2015.
- Dave, A. C. and Lozier, M. S.: Examining the global record of interannual variability in stratification and marine productivity in the low-latitude and mid-latitude ocean, *J. Geophys. Res. Oceans*, 118, 3114–3127, <https://doi.org/10.1002/jgrc.20224>, 2013.
- 1145 Dave, A. C. and Lozier, M. S.: The impact of advection on stratification and chlorophyll variability in the equatorial Pacific, *Geophys. Res. Lett.*, 42, 4523–4531, <https://doi.org/10.1002/2015GL063290>, 2015.
- De Dominicis, M., Wolf, J., and O'Hara Murray, R.: Comparative Effects of Climate Change and Tidal Stream Energy Extraction in a Shelf Sea, *J. Geophys. Res. Oceans*, 123, 5041–5067, <https://doi.org/10.1029/2018JC013832>, 2018.
- 1150 Detoni, A. M. S., de Souza, M. S., Garcia, C. A. E., Tavano, V. M., and Mata, M. M.: Environmental conditions during phytoplankton blooms in the vicinity of James Ross Island, east of the Antarctic Peninsula, *Polar Biol.*, 38, 1111–1127, <https://doi.org/10.1007/s00300-015-1670-7>, 2015.
- Diehl, S.: Phytoplankton, Light, and Nutrients in a Gradient of Mixing Depths: Theory, *Ecology*, 83, 386–398, [https://doi.org/10.1890/0012-9658\(2002\)083\[0386:PLANIA\]2.0.CO;2](https://doi.org/10.1890/0012-9658(2002)083[0386:PLANIA]2.0.CO;2), 2002.
- 1155 Diehl, S., Berger, S., Ptacnik, R., and Wild, A.: Phytoplankton, Light, and Nutrients in a Gradient of Mixing Depths: Field Experiments, *Ecology*, 83, 399–411, [https://doi.org/10.1890/0012-9658\(2002\)083\[0399:PLANIA\]2.0.CO;2](https://doi.org/10.1890/0012-9658(2002)083[0399:PLANIA]2.0.CO;2), 2002.
- [Dorrell, R. M., Lloyd, C. J., Lincoln, B. J., Rippeth, T. P., Taylor, J. R., Caulfield, C. P., Sharples, J., Polton, J. A., Scannell, B. D., Greaves, D. M., Hall, R. A., and Simpson, J. H.: Anthropogenic Mixing in Seasonally Stratified Shelf Seas by Offshore Wind Farm Infrastructure, \*Front. Mar. Sci.\*, 9, 2022.](#)
- 1160 D'Ortenzio, F., Lavigne, H., Besson, F., Claustre, H., Coppola, L., Garcia, N., Laës-Huon, A., Le Reste, S., Malardé, D., Migon, C., Morin, P., Mortier, L., Poteau, A., Prieur, L., Raimbault, P., and Testor, P.: Observing mixed layer depth, nitrate and chlorophyll concentrations in the northwestern Mediterranean: A combined satellite and NO<sub>3</sub> profiling floats experiment, *Geophys. Res. Lett.*, 41, 6443–6451, <https://doi.org/10.1002/2014GL061020>, 2014.
- 1165

ha formattato: Tipo di carattere: +Corpo (Calibri), 11 pt

- Ducklow, H. W., Baker, K., Martinson, D. G., Quetin, L. B., Ross, R. M., Smith, R. C., Stammerjohn, S. E., Vernet, M., and Fraser, W.: Marine pelagic ecosystems: the West Antarctic Peninsula, *Philos. Trans. R. Soc. B Biol. Sci.*, 362, 67–94, <https://doi.org/10.1098/rstb.2006.1955>, 2007.
- 1170 Durán-Campos, E., Monreal-Gómez, M. A., Salas de León, D. A., and Coria-Monter, E.: Chlorophyll-a vertical distribution patterns during summer in the Bay of La Paz, Gulf of California, Mexico, *Egypt. J. Aquat. Res.*, 45, 109–115, <https://doi.org/10.1016/j.ejar.2019.04.003>, 2019.
- Durski, S. M., Glenn, S. M., and Haidvogel, D. B.: Vertical mixing schemes in the coastal ocean: Comparison of the level 2.5 Mellor-Yamada scheme with an enhanced version of the K profile parameterization, *J. Geophys. Res. Oceans*, 109, <https://doi.org/10.1029/2002JC001702>, 2004.
- 1175 ~~EMODnet Bathymetry Consortium: EMODnet Digital Bathymetry (DTM), 2018.~~
- Erickson, Z. K., Thompson, A. F., Cassar, N., Sprintall, J., and Mazloff, M. R.: An advective mechanism for deep chlorophyll maxima formation in southern Drake Passage, *Geophys. Res. Lett.*, 43, 10,846–10,855, <https://doi.org/10.1002/2016GL070565>, 2016.
- 1180 Gielen, D., Gorini, R., Wagner, N., Leme, R., Gutierrez, L., Prakash, G., Asmelash, E., Janeiro, L., Gallina, G., Vale, G., Sani, L., Casals, X. G., Ferroukhi, R., Parajuli, B., Feng, J., Alexandri, E., Chewpreecha, U., Goldman, M., Heald, S., Stenning, J., Pollitt, H., García-Bañños, C., and Renner, M.: Global energy Transformation: A Roadmap to 2050, 2019.
- Glorioso, P. D. and Simpson, J. H.: Numerical modelling of the M2 tide on the northern Patagonian Shelf, *Cont. Shelf Res.*, 14, 267–278, [https://doi.org/10.1016/0278-4343\(94\)90016-7](https://doi.org/10.1016/0278-4343(94)90016-7), 1994.
- 1185 ~~Goebel, N. L., Frolov, S., and Edwards, C. A.: Complementary use of Wave Glider and satellite measurements: Description of spatial decorrelation scales in Chl-a fluorescence across the Pacific basin, *Methods Oceanogr.*, 10, 90–103, <https://doi.org/10.1016/j.mio.2014.07.001>, 2014.~~
- González-Pola, C., Fernández-Díaz, J. M., and Lavín, A.: Vertical structure of the upper ocean from profiles fitted to physically consistent functional forms, *Deep Sea Res. Part Oceanogr. Res. Pap.*, 54, 1985–2004, <https://doi.org/10.1016/j.dsr.2007.08.007>, 2007.
- 1190 Gradone, J. C., Oliver, M. J., Davies, A. R., Moffat, C., and Irwin, A.: Sea Surface Kinetic Energy as a Proxy for Phytoplankton Light Limitation in the Summer Pelagic Southern Ocean, *J. Geophys. Res. Oceans*, 125, e2019JC015646, <https://doi.org/10.1029/2019JC015646>, 2020.
- 1195 ~~Hastie, T. J., and Tibshirani, R. J.: *Generalized additive models*. 1<sup>st</sup> edition, Routledge, <https://doi.org/10.1201/9780203753781>, 1990.~~
- Hickman, A., Moore, C., Sharples, J., Lucas, M., Tilstone, G., Krivtsov, V., and Holligan, P.: Primary production and nitrate uptake within the seasonal thermocline of a stratified shelf sea, *Mar. Ecol. Prog. Ser.*, 463, 39–57, <https://doi.org/10.3354/meps09836>, 2012.
- 1200 Höfer, J., Giesecke, R., Hopwood, M. J., Carrera, V., Alarcón, E., and González, H. E.: The role of water column stability and wind mixing in the production/export dynamics of two bays in the Western Antarctic Peninsula, *Prog. Oceanogr.*, 174, 105–116, <https://doi.org/10.1016/j.pocean.2019.01.005>, 2019.
- Holligan, P. M., Balch, W. M., and Yentsch, C. M.: The significance of subsurface chlorophyll, nitrite and ammonium maxima in relation to nitrogen for phytoplankton growth in stratified waters of the Gulf of Maine, *J. Mar. Res.*, 42, 1051–1073, <https://doi.org/10.1357/002224084788520747>, 1984.
- 1205 Holte, J. and Talley, L.: A New Algorithm for Finding Mixed Layer Depths with Applications to Argo Data and Subantarctic Mode Water Formation, *J. Atmospheric Ocean. Technol.*, 26, 1920–1939, <https://doi.org/10.1175/2009JTECHO543.1>, 2009.

ha formattato: Tipo di carattere: +Corpo (Calibri), 11 pt

ha formattato: Tipo di carattere: +Corpo (Calibri), 11 pt

ha formattato: Tipo di carattere: +Corpo (Calibri), 11 pt

- Huisman, J., Arrayás, M., Ebert, U., and Sommeijer, B.: How do sinking phytoplankton species manage to persist?, *Am. Nat.*, 159, 245–254, <https://doi.org/10.1086/338511>, 2002.
- 1210 Jones, S. E., Jago, C. F., Bale, A. J., Chapman, D., Howland, R. J. M., and Jackson, J.: Aggregation and resuspension of suspended particulate matter at a seasonally stratified site in the southern North Sea: physical and biological controls, *Cont. Shelf Res.*, 18, 1283–1309, [https://doi.org/10.1016/S0278-4343\(98\)00044-2](https://doi.org/10.1016/S0278-4343(98)00044-2), 1998.
- Kara, A. B., Rochford, P. A., and Hurlburt, H. E.: An optimal definition for ocean mixed layer depth, *J. Geophys. Res. Oceans*, 105, 16803–16821, <https://doi.org/10.1029/2000JC900072>, 2000.
- 1215 Klymak, J. M., Pinkel, R., and Rainville, L.: Direct Breaking of the Internal Tide near Topography: Kaena Ridge, Hawaii, *J. Phys. Oceanogr.*, 38, 380–399, <https://doi.org/10.1175/2007JPO3728.1>, 2008.
- Lande, R. and Wood, A. M.: Suspension times of particles in the upper ocean, *Deep Sea Res. Part Oceanogr. Res. Pap.*, 34, 61–72, [https://doi.org/10.1016/0198-0149\(87\)90122-1](https://doi.org/10.1016/0198-0149(87)90122-1), 1987.
- 1220 Lavigne, H., D’Ortenzio, F., Ribera D’Alcalá, M., Claustre, H., Sauzède, R., and Gacic, M.: On the vertical distribution of the chlorophyll *a* concentration in the Mediterranean Sea: a basin-scale and seasonal approach, *Biogeosciences*, 12, 5021–5039, <https://doi.org/10.5194/bg-12-5021-2015>, 2015.
- Lee, Z., Marra, J., Perry, M. J., and Kahru, M.: Estimating oceanic primary productivity from ocean color remote sensing: A strategic assessment, *J. Mar. Syst.*, 149, 50–59, <https://doi.org/10.1016/j.jmarsys.2014.11.015>, 2015.
- 1225 Leeuwen, S. van, Tett, P., Mills, D., and Molen, J. van der: Stratified and nonstratified areas in the North Sea: Long-term variability and biological and policy implications, *J. Geophys. Res. Oceans*, 120, 4670–4686, <https://doi.org/10.1002/2014JC010485>, 2015.
- Lévy, M., Jahn, O., Dutkiewicz, S., Follows, M. J., and d’Ovidio, F.: The dynamical landscape of marine phytoplankton diversity, *J. R. Soc. Interface*, 12, 20150481, <https://doi.org/10.1098/rsif.2015.0481>, 2015.
- 1230 Lips, U., Lips, I., Liblik, T., and Kuvaldina, N.: Processes responsible for the formation and maintenance of sub-surface chlorophyll maxima in the Gulf of Finland, *Estuar. Coast. Shelf Sci.*, 88, 339–349, <https://doi.org/10.1016/j.ecss.2010.04.015>, 2010.
- Lloyd, S.: Least-squares quantization in PCM, in: *IEEE Transactions on Information Theory*, 28 (2), 129–137, <https://ieeexplore.ieee.org/document/1056489>, 1982.
- 1235 Loder, J. W., Brickman, D., and Horne, E. P. W.: Detailed structure of currents and hydrography on the northern side of Georges Bank, *J. Geophys. Res. Oceans*, 97, 14331–14351, <https://doi.org/10.1029/92JC01342>, 1992.
- Lorbacher, K., Dommenges, D., Niiler, P. P., and Köhl, A.: Ocean mixed layer depth: A subsurface proxy of ocean-atmosphere variability, *J. Geophys. Res. Oceans*, 111, <https://doi.org/10.1029/2003JC002157>, 2006.
- 1240 Lozier, M. S., Dave, A. C., Palter, J. B., Gerber, L. M., and Barber, R. T.: On the relationship between stratification and primary productivity in the North Atlantic, *Geophys. Res. Lett.*, 38, <https://doi.org/10.1029/2011GL049414>, 2011.
- Martin, A. P.: Phytoplankton patchiness: the role of lateral stirring and mixing, *Prog. Oceanogr.*, 57, 125–174, [https://doi.org/10.1016/S0079-6611\(03\)00085-5](https://doi.org/10.1016/S0079-6611(03)00085-5), 2003.
- 1245 Martin, J., Tremblay, J.-É., Gagnon, J., Tremblay, G., Lapoussière, A., Jose, C., Poulin, M., Gosselin, M., Gratton, Y., and Michel, C.: Prevalence, structure and properties of subsurface chlorophyll maxima in Canadian Arctic waters, *Mar. Ecol. Prog. Ser.*, 412, 69–84, <https://doi.org/10.3354/meps08666>, 2010.

ha formattato: Tipo di carattere: +Corpo (Calibri), 11 pt

ha formattato: Tipo di carattere: +Corpo (Calibri), 11 pt

ha formattato: Tipo di carattere: +Corpo (Calibri), 11 pt

ha formattato: Tipo di carattere: +Corpo (Calibri), 11 pt

ha formattato: Tipo di carattere: +Corpo (Calibri), 11 pt

- 1250 [Mignot, A., Claustre, H., D&apos;Ortenzio, F., Xing, X., Poteau, A., and Ras, J.: From the shape of the vertical profile of in vivo fluorescence to Chlorophyll \*a\* concentration, \*Biogeosciences\*, 8, 2391–2406, <https://doi.org/10.5194/bg-8-2391-2011>, 2011.](#)
- [van der Molen, J., Smith, H. C. M., Lepper, P., Limpenny, S., and Rees, J.: Predicting the large-scale consequences of offshore wind turbine array development on a North Sea ecosystem, \*Cont. Shelf Res.\*, 85, 60–72, <https://doi.org/10.1016/j.csr.2014.05.018>, 2014.](#)
- 1255 [Montégut, C. de B., Madec, G., Fischer, A. S., Lazar, A., and Iudicone, D.: Mixed layer depth over the global ocean: An examination of profile data and a profile-based climatology, \*J. Geophys. Res. Oceans\*, 109, <https://doi.org/10.1029/2004JC002378>, 2004.](#)
- 1260 [Montes-Hugo, M., Doney, S. C., Ducklow, H. W., Fraser, W., Martinson, D., Stammerjohn, S. E., and Schofield, O.: Recent Changes in Phytoplankton Communities Associated with Rapid Regional Climate Change Along the Western Antarctic Peninsula, \*Science\*, 323, 1470–1473, <https://doi.org/10.1126/science.1164533>, 2009.](#)
- [Neill, S. P. and Hashemi, M. R.: Tidal Energy, in: \*Fundamentals of Ocean Renewable Energy\*, Elsevier, 47–81, <https://doi.org/10.1016/B978-0-12-810448-4.00003-3>, 2018.](#)
- 1265 [Orihuela-Pinto, B., England, M. H., and Taschetto, A. S.: Interbasin and interhemispheric impacts of a collapsed Atlantic Overturning Circulation, \*Nat. Clim. Change\*, 12, 558–565, <https://doi.org/10.1038/s41558-022-01380-y>, 2022.](#)
- [Pingree, R. D., Holligan, P. M., Mardell, G. T., and Harris, R. P.: Vertical distribution of plankton in the skagerrak in relation to doming of the seasonal thermocline, \*Cont. Shelf Res.\*, 1, 209–219, \[https://doi.org/10.1016/0278-4343\\(82\\)90005-X\]\(https://doi.org/10.1016/0278-4343\(82\)90005-X\), 1982.](#)
- 1270 [Prend, C. J., Gille, S. T., Talley, L. D., Mitchell, B. G., Rosso, I., and Mazloff, M. R.: Physical Drivers of Phytoplankton Bloom Initiation in the Southern Ocean's Scotia Sea, \*J. Geophys. Res. Oceans\*, 124, 5811–5826, <https://doi.org/10.1029/2019JC015162>, 2019.](#)
- [Prézelin, B. B., Hofmann, E. E., Mengelt, C., and Klinck, J. M.: The linkage between Upper Circumpolar Deep Water \(UCDW\) and phytoplankton assemblages on the west Antarctic Peninsula continental shelf, \*J. Mar. Res.\*, 58, 165–202, <https://doi.org/10.1357/002224000321511133>, 2000.](#)
- 1275 [Prézelin, B. B., Hofmann, E. E., Moline, M., and Klinck, J. M.: Physical forcing of phytoplankton community structure and primary production in continental shelf waters of the Western Antarctic Peninsula, \*J. Mar. Res.\*, 62, 419–460, <https://doi.org/10.1357/0022240041446173>, 2004.](#)
- [R Core Team: \*R Foundation for Statistical Computing\*. Vienna, Austria, 2018.](#)
- 1280 [Richardson, K. and Bendtsen, J.: Vertical distribution of phytoplankton and primary production in relation to nutricline depth in the open ocean, \*Mar. Ecol. Prog. Ser.\*, 620, 33–46, <https://doi.org/10.3354/meps12960>, 2019.](#)
- [Richardson, K. and Pedersen, F. B.: Estimation of new production in the North Sea: consequences for temporal and spatial variability of phytoplankton, \*ICES J. Mar. Sci.\*, 55, 574–580, <https://doi.org/10.1006/jmsc.1998.0402>, 1998.](#)
- 1285 [Rosenberg, R., Dahl, E., Edler, L., Fyrberg, L., Granéli, E., Granéli, W., Hagström, Å., Lindahl, O., Matos, M. O., Pettersson, K., Sahlsten, E., Tiselius, P., Turk, V., and Wikner, J.: Pelagic nutrient and energy transfer during spring in the open and coastal Skagerrak, \*Mar. Ecol. Prog. Ser.\*, 61, 215–231, 1990.](#)
- [Ross, O. N. and Sharples, J.: Phytoplankton motility and the competition for nutrients in the thermocline, \*Mar. Ecol. Prog. Ser.\*, 347, 21–38, <https://doi.org/10.3354/meps06999>, 2007.](#)

ha formattato: Tipo di carattere: +Corpo (Calibri), 11 pt

ha formattato: Tipo di carattere: +Corpo (Calibri), 11 pt

ha formattato: Tipo di carattere: +Corpo (Calibri), 11 pt

1290 Ryan-Keogh, T. J. and Thomalla, S. J.: Deriving a Proxy for Iron Limitation From Chlorophyll Fluorescence on Buoyancy Gliders, *Front. Mar. Sci.*, 7, 275, <https://doi.org/10.3389/fmars.2020.00275>, 2020.

Schmidt, K., Birchill, A. J., Atkinson, A., Brewin, R. J. W., Clark, J. R., Hickman, A. E., Johns, D. G., Lohan, M. C., Milne, A., Pardo, S., Polimene, L., Smyth, T. J., Tarran, G. A., Widdicombe, C. E., Woodward, E. M. S., and Ussher, S. J.: Increasing picocyanobacteria success in shelf waters contributes to long-term food web degradation, *Glob. Change Biol.*, <https://doi.org/10.1111/gcb.15161>, 2020.

Schofield, O., Miles, T., Alderkamp, A.-C., Lee, S., Haskins, C., Rogalsky, E., Sipler, R., Sherrell, R. M., and Yager, P. L.: *In situ* phytoplankton distributions in the Amundsen Sea Polynya measured by autonomous gliders, *Elem. Sci. Anthr.*, 3, 000073, <https://doi.org/10.12952/journal.elementa.000073>, 2015.

1300 [Schulien, J. A., Behrenfeld, M. J., Hair, J. W., Hostetler, C. A., and Twardowski, M. S.: Vertically- resolved phytoplankton carbon and net primary production from a high spectral resolution lidar, \*Opt. Express\*, 25, 13577, <https://doi.org/10.1364/OE.25.013577>, 2017.](#)

[Schultze, L. K. P., Merckelbach, L. M., Horstmann, J., Raasch, S., and Carpenter, J. R.: Increased Mixing and Turbulence in the Wake of Offshore Wind Farm Foundations, \*J. Geophys. Res. Oceans\*, 125, e2019JC015858, <https://doi.org/10.1029/2019JC015858>, 2020.](#)

1305 [Scott, B. E., Sharples, J., Ross, O. N., Wang, J., Pierce, G. J., and Camphuysen, C. J.: Sub-surface hotspots in shallow seas: fine-scale limited locations of top predator foraging habitat indicated by tidal mixing and sub-surface chlorophyll, \*Mar. Ecol. Prog. Ser.\*, 408, 207–226, <https://doi.org/10.3354/meps08552>, 2010.](#)

ha formattato: Tipo di carattere: +Corpo (Calibri), 11 pt

1310 [Sharples, J., Moore, M. C., Rippeth, T. P., Holligan, P. M., Hydes, D. J., Fisher, N. R., and Simpson, J. H.: Phytoplankton distribution and survival in the thermocline, \*Limnol. Oceanogr.\*, 46, 486–496, <https://doi.org/10.4319/lo.2001.46.3.0486>, 2001.](#)

[Sharples, J., Ross, O. N., Scott, B. E., Greenstreet, S. P. R., and Fraser, H.: Inter-annual variability in the timing of stratification and the spring bloom in the North-western North Sea, \*Cont. Shelf Res.\*, 26, 733–751, <https://doi.org/10.1016/j.csr.2006.01.011>, 2006.](#)

1315 [Sharples, J., Scott, B. E., and Inall, M. E.: From physics to fishing over a shelf sea bank, \*Prog. Oceanogr.\*, 117, 1–8, <https://doi.org/10.1016/j.pocean.2013.06.015>, 2013.](#)

[Silva, E., Counillon, F., Brajard, J., Korosov, A., Pettersson, L. H., Samuelsen, A., and Keenlyside, N.: Twenty-One Years of Phytoplankton Bloom Phenology in the Barents, Norwegian, and North Seas, \*Front. Mar. Sci.\*, 8, 2021.](#)

1320 [Simpson, J., Hughes, D. G., and Morris, N. C. G.: The relation of seasonal stratification to tidal mixing on the continental shelf, \*Deep-Sea Res.\*, 327–340, 1980.](#)

ha formattato: Tipo di carattere: +Corpo (Calibri), 11 pt

[Somavilla, R., González-Pola, C., and Fernández-Díaz, J.: The warmer the ocean surface, the shallower the mixed layer. How much of this is true?, \*J. Geophys. Res. Oceans\*, 122, 7698–7716, <https://doi.org/10.1002/2017JC013125>, 2017.](#)

1325 [Sverdrup, H. U.: On conditions for the vernal blooming of phytoplankton. \*J. Cons. Int. Explor. Mer.\*, 18, 287–295, 1953.](#)

[Steinacher, M., Joos, F., Frölicher, T. L., Bopp, L., Cadule, P., Cocco, V., Doney, S. C., Gehlen, M., Lindsay, K., Moore, J. K., Schneider, B., and Segschneider, J.: Projected 21st century decrease in marine productivity: a multi-model analysis, \*Biogeosciences\*, 7, 979–1005, <https://doi.org/10.5194/bg-7-979-2010>, 2010.](#)

1330 [Taboada, F. G. and Anadón, R.:](#) Patterns of change in sea surface temperature in the North Atlantic during the last three decades: beyond mean trends, *Clim. Change*, 115, 419–431, <https://doi.org/10.1007/s10584-012-0485-6>, 2012.

ha formattato: Tipo di carattere: +Corpo (Calibri), 11 pt

Takahashi, M. and Hori, T.: Abundance of picophytoplankton in the subsurface chlorophyll maximum layer in subtropical and tropical waters, *Mar. Biol.*, 79, 177–186, <https://doi.org/10.1007/BF00951826>, 1984.

1335 Therriault, J.-C., Lawrence, D. J., and Piatt, T.: Spatial variability of phytoplankton turnover in relation to physical processes in a coastal environment, *Limnol. Oceanogr.*, 23, 900–911, <https://doi.org/10.4319/lo.1978.23.5.0900>, 1978.

[Thomson, R. E. and Fine, I. V.:](#) Estimating Mixed Layer Depth from Oceanic Profile Data, *J. Atmospheric Ocean. Technol.*, 20, 319–329, [https://doi.org/10.1175/1520-0426\(2003\)020<0319:EMLDFO>2.0.CO;2](https://doi.org/10.1175/1520-0426(2003)020<0319:EMLDFO>2.0.CO;2), 2003.

1340 [Trifonova, N. I., Scott, B. E., De Dominicis, M., Waggitt, J. J., and Wolf, J.:](#) Bayesian network modelling provides spatial and temporal understanding of ecosystem dynamics within shallow shelf seas, *Ecol. Indic.*, 129, 107997, <https://doi.org/10.1016/j.ecolind.2021.107997>, 2021.

ha formattato: Tipo di carattere: +Corpo (Calibri), 11 pt

1345 [Uitz, J., Claustre, H., Morel, A., and Hooker, S. B.:](#) Vertical distribution of phytoplankton communities in open ocean: An assessment based on surface chlorophyll, *J. Geophys. Res.-Oceans*, 111, <https://doi.org/10.1029/2005JC003207>, 2006.

[Walsby, A. E.:](#) Numerical integration of phytoplankton photosynthesis through time and depth in a water column, *New Phytol.*, 136, 189–209, <https://doi.org/10.1046/j.1469-8137.1997.00736.x>, 1997.

ha formattato: Tipo di carattere: +Corpo (Calibri), 11 pt

Warton, D. I., Wright, I. J., Falster, D. S., and Westoby, M.: Bivariate line-fitting methods for allometry, *Biol. Rev.*, 81, 259–291, <https://doi.org/10.1017/S1464793106007007>, 2006.

1350 Weston, K., Fernand, L., Mills, D. K., Delahunty, R., and Brown, J.: Primary production in the deep chlorophyll maximum of the central North Sea, *J. Plankton Res.*, 27, 909–922, <https://doi.org/10.1093/plankt/fbi064>, 2005.

Yentsch, C. S.: Influence of geostrophy on primary production. [Effect of ocean currents on nutrients of ocean water], *Tethys Fr.*, 6:1–2, 1974.

1355 Yentsch, C. S.: Phytoplankton Growth in the Sea, in: *Primary Productivity in the Sea*, edited by: Falkowski, P. G., Springer US, Boston, MA, 17–32, [https://doi.org/10.1007/978-1-4684-3890-1\\_2](https://doi.org/10.1007/978-1-4684-3890-1_2), 1980.

Zhang, W.-Z., Wang, H., Chai, F., and Qiu, G.: Physical drivers of chlorophyll variability in the open South China Sea, *J. Geophys. Res.-Oceans*, 121, 7123–7140, <https://doi.org/10.1002/2016JC011983>, 2016.

1360 Zhao, C., Maerz, J., Hofmeister, R., Röttgers, R., Wirtz, K., Riethmüller, R., and Schrum, C.: Characterizing the vertical distribution of chlorophyll a in the German Bight, *Cont. Shelf Res.*, 175, 127–146, <https://doi.org/10.1016/j.csr.2019.01.012>, 2019a.

Zhao, C., Daewel, U., and Schrum, C.: Tidal impacts on primary production in the North Sea, *Earth Syst. Dyn.*, 10, 287–317, <https://doi.org/10.5194/esd-10-287-2019>, 2019b.